SIAM REVIEW
Vol. 20, No. 2, April 1978

COCHLEAR DYNAMICS: THE EVOLUTION OF A MATHEMATICAL MODEL*

A. INSELBERG†

Dedicated to Professor Heinz von Foerster on the Occasion of his Retirement

Abstract. The evolution of a mathematical model designed to clarify the relationship between the structure and the function of the cochlea (inner ear) is traced. Starting from physical (rather than empirical) considerations, the mathematical description of each model is derived in terms of well-defined physical properties of the cochlea. Initially, the basilar membrane is modeled as a uniform simply supported beam vibrating in a viscous medium, and driven by a concentrated oscillating moment at the basal end. In such a system traveling and standing waves (transients) occur simultaneously. An analysis of the traveling waves reveals a place principle. The model has high and low frequency "thresholds" (i.e., at very high and very low frequencies, frequency discrimination diminishes). The model suggests that the fluid properties play a particularly important role at high frequencies, while the role of cochlear geometry becomes dominant at low frequencies. In the second stage, the beam is enclosed in a rectangular "cochlea" divided into two equal chambers and filled with viscous and incompressible fluid (the perilymph) communicating through a small opening at one end (the helicotrema). At the opposite end, the system is driven by a piston-like periodic forcing (i.e., the movement of the stapes in the middle ear). It is assumed that the oscillations of the basilar membrane have long wavelength—compared with the cochlear chamber height—and that a thin unsteady boundary layer forms on all surfaces within the cochlea. In general, the results confirm and improve the results of the previous model. The place principle exhibited by this model corresponds well with experimental data at higher frequencies, but not at low frequencies. For good low frequency response, the model must be endowed with much of the cochlea's intricate geometry. This is done in the third model where the basilar membrane is represented by a wedge-shaped isotropic plate of constant thickness and enclosed by an arbitrary surface of revolution representing the cochlear shell. The plate is simply supported along its long edges while three different boundary conditions are considered for the support at the helicotrema. So as to emulate the presence of the cochlear duct (third cochlear chamber), a pressure difference in the fluid at the helicotrema is included. As in the second model, the cochlear fluids are taken to be viscous and incompressible, and the system is driven by periodic forcing at one end. The solution of the equations of motion as the input frequency tends to zero is obtained. The role of the basilar membrane taper, as well as cochlear cross-section's opposing taper, is delimited. The third chamber (cochlear duct) must be included in the model in order to utilize the full length of the basilar membrane for frequency discrimination. Consequently, the boundary conditions of the basilar membrane at the helicotrema can be analyzed, and it is shown that an elastic support (representing a "ligament") is required at the helicotrema.

An annotated selective survey of cochlea modeling since 1869 is provided. Some research problems conclude the narrative.

CONTENTS

* Received by the editors August 18, 1975, and in revised form December 23, 1976.

† Los Angeles Scientific Center, IBM, Los Angeles, California 90045. Now at Department of Mathematics, Ben Gurion University of the Negev, Beersheva, Israel.

0. Preliminaries.

0.1. Overview and a little history. Over a century ago, Helmholtz constructed elegant mathematical models in his investigations of hearing [1] and vision [2]. Interest in mathematical modeling in the biosciences regenerated with the publication of *Elements of Physical Biology* [3], a wonderfully readable book by Lotka, which was soon followed by Volterra's classical work in mathematical ecology [4] and Rashevsky's seminal *Mathematical Biophysics* [5]. A measure of the modern attainment is given by Resnikoff's elegant model of color perception [6] and Thom's mathematical theory of morphogenesis [7] (see also Zeeman [8]). (Swan [9] presents an extensive current bibliography of mathematical biology.) Thom's work was motivated by studies in the local topological properties of differentiable mappings [10], [11] (see also Callahan [12]). Work in the cognitive processes by McCulloch and Pitts [13], [14] and by von Foerster [15] motivated the search for superposition principles for nonlinear operators [16], [17]. Numerous books and no fewer than seven journals[1] attest to the growing cross-fertilization between the biosciences and mathematics.

The form of a mathematical model depends upon two considerations: representational adequacy and mathematical tractability. Representational adequacy, in turn, is determined by the model's purpose. Strikingly different models of the same system may be constructed to emphasize different aspects of that system. We develop a mathematical model designed to clarify the relationship between the structure and the function of the cochlea of the inner ear. This model evolves through three stages, each more accurately representing the cochlea. At each stage, comparisons between experimental evidence and the model's predictions suggest appropriate changes for the subsequent reformulation.

0.2. The anatomy and physiology of the ear [1], [18]–[28]**.** The ear is conveniently subdivided into three parts—outer, middle, and inner ear (Fig. 1.). The outer ear consists of the external flap and the ear canal leading to the drum (i.e., tympanic) membrane of the middle ear. Attached to this membrane is a chain of three small bones called the middle ear ossicles. The innermost ossicle, called stapes, has its footplate implanted at the oval window of the inner ear.

The auditory portion of the inner ear is a snail-shaped structure called the cochlea. With the exception of an initial bulge at the basal end, where the stapes is embedded, the cochlea narrows gradually towards its apex (apical end). In man, it winds about $2\frac{3}{4}$ turns and its uncoiled legth is about 35 mm. The cochlea (Fig. 2) is composed of three fluid-filled chambers (scala tympani, scala vestibuli, and scala media). The sense organ proper, i.e., the organ of Corti with its accessory structures, is contained in the scala media (also called the cochlear duct), and is supported by the fibrous basilar membrane that forms part of one wall of the cochlear duct (Fig. 3). The

[1] *Biophysical Journal*; *Bulletin of Mathematical Biophysics*; *Computers and Biomedical Research*; *Journal of Mathematical Biology*; *Journal of Theoretical Biology*; *Mathematical Biosciences*; *Progress in Biophysics and Biophysical Chemistry*.

thin and pliant Reissner's membrane separates the cochlear duct from the scala vestibuli which, at the basal end of the cochlea, communicates with the middle ear through the oval window. The scala tympani ends at the round window, an opening on the cochlear wall covered by a membrane. The cochlear duct, formed by the basilar

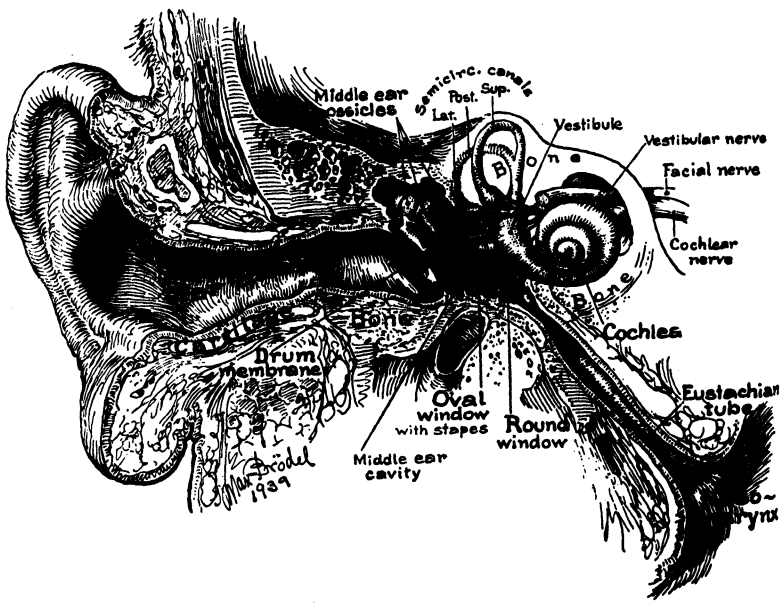

FIG. 1. *Schematic of the ear, the cochlea is rotated somewhat from the normal orientation to show its coils more clearly. From "3 Unpublished Drawings of the Anatomy of the Human Ear," by Max Brodel. Copyright* 1946. *W. B. Saunders Co., Philadelphia. Used by permission.*

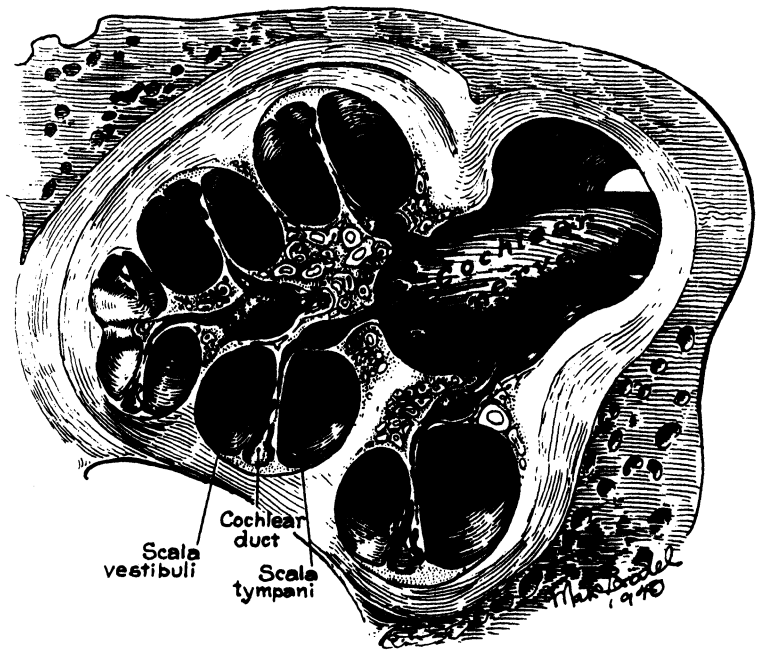

FIG. 2. *Cochlear cross section. From "Year Book of Eye, Ear, Nose and Throat," by L. Bothman and S. J. Crowe, eds. Copyright* 1940. *Year Book Medical Publisher, Inc., Chicago. Used by permission.*

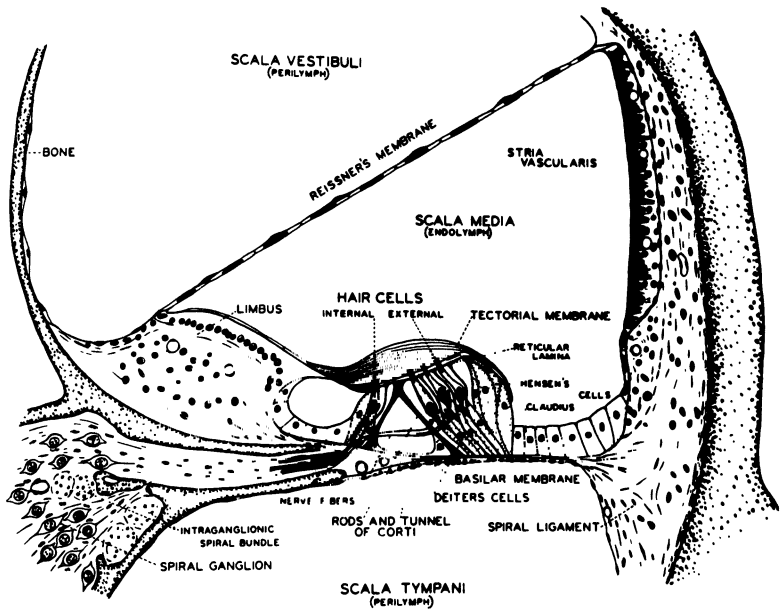

FIG. 3. *Cross section of the cochlear duct. From "Acoustic Trauma in the Guinea Pig," H. Davis and Associates in J. Acoust. Soc. of Amer.* 1953. *Used by permission.*

membrane and its supports and Reissner's membrane, ends "blindly" just short of the cochlear apex, leaving a small opening called the helicotrema. This opening allows the scala tympani to communicate with the scala vestibuli (see Figs. 9, 13 and 19). The sensory surface of the spiral cochlea, then, is contained in the cochlear duct, a relatively narrow fluid-filled tube, separating two communicating fluid-filled chambers.

Hearing results from two kinds of processes, one mechanical and the other electro-chemical. The sound signal is conducted via the outer and middle ear to the cochlear fluids, which in turn force the basilar membrane to oscillate. These are the mechanical events in the auditory process (Fig. 4). While the conductive mechanism is relatively well understood, the manifestation of the acoustical information in terms of the motion of the basilar membrane is not. Direct experimental measurements of cochlear function are difficult to obtain due to the inaccessibility of the cochlea and the delicate structure of the basilar membrane. Consequently, modeling is a particularly useful tool, and many models (mechanical [29]–[36], electrical [37]–[45] and mathematical [46]–[80]) have been developed (see Appendix). Difficulties notwithstanding, experimental data on the function of the cochlea has been painstakingly and ingeniously obtained. Using stroboscopic techniques, von Békésy [22] obtained extensive data. Subsequently, the Mössbauer effect (Johnstone and Boyle [81], Rhode [82], and Robles, Rhode and Geisler [83]), spectral interferometry (Kohllöffel [84]), and the capacitive probe technique (Wilson and Johnstone [85]) have been used to obtain data on the displacement patterns of the basilar membrane. The interpretation of the data, however, is often problematical and remains controversial. For reviews of the data and its interpretation see Wilson [86] and Zwislocki [87]. Geisler and Hubbard [88] comment on the compatibility of measurements. In formulating cochlea models, the following observations based primarily on von Békésy's experiments are particularly useful:

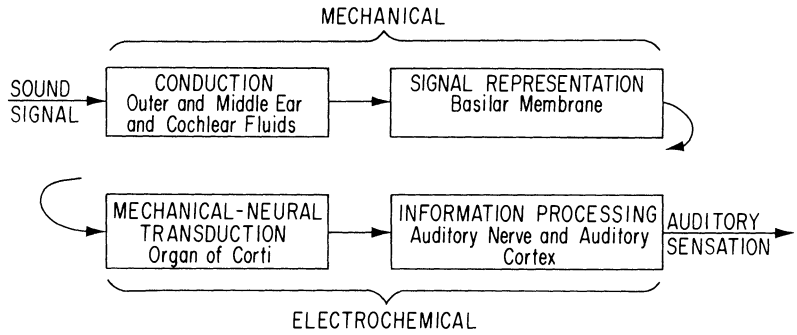

FIG. 4. *Sequence of auditory events.*

(a) The basilar membrane has neither longitudinal nor transverse tension in the resting state.

(b) The stiffness of the basilar membrane decreases by about two orders of magnitude from the stapes to the helicotrema; the tapered shape of the membrane can account for this. The basilar membrane exhibits uniform elastic properties throughout (i.e., it is isotropic). By contrast, recently Novoselova [75] concluded that the basilar membrane is anisotropic.

(c) The damping of basilar membrane motion due to the cochlear fluid is essentially constant at all points on the membrane except near the helicotrema where it increases.

(d) Traveling waves exist in the motion of the basilar membrane for excitation frequencies above 25 cps.

(e) There is a Place Principle—i.e., there exists a one-to-one correspondence between excitation frequencies and positions of the maximum membrane displacement. Low frequencies result in maxima close to the helicotrema and high frequencies produce maxima near the stapes (see Fig. 5).

For data, both measured and inferred, on the basilar membrane and cochlea, see the tables in [69] and the Appendix in [20].

In the wake of von Békésy's observations, several mathematical models of the basilar membrane were devised. Generally, the basilar membrane was modeled as an array of uncoupled mass-spring-damped (msd) elements though von Békésy's measurements imply that adjacent basilar membrane elements are coupled. The motion of such a system is described by a second order differential equation whose spatially dependent coefficients are determined by the physical properties and mass distribution of the msd elements. Since such equations have a very rich class of solution functions, it is not surprising that von Békésy's observations could be matched—by the various models—with "appropriate" choices of coefficients corresponding to properties of the msd array.

In order the understand the effects of lateral elastic coupling, a study was initiated in 1959, under the direction of von Foerster [89] where the basilar membrane was modeled as a stiff one-dimensional body oscillating in a viscous medium. That work resulted in a simple model [62] derived from first principles, and provided the first stage in the development of the present model (§ 1). In the second stage [76], [77], a careful treatment of cochlear fluid mechanics is introduced (§ 2). Finally [80], the model is modified to include the variable geometry of the cochlea and the basilar membrane (§ 3).

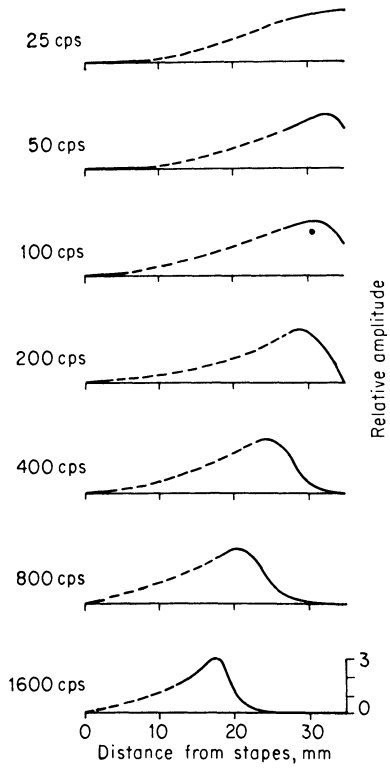

FIG. 5. *The place principle at low frequencies. The maximum of the time-envelope of the basilar membrane's oscillations shifts towards the stapes (basal end) with increasing frequency. Data obtained by G. von Békésy from a cadaver specimen. Solid portions indicate measurements and dotted portions of the curves are interpolations. From "Experiments in Hearing," by G. von Békésy. Copyright* 1960, *McGraw-Hill, Inc., New York. Used by permission.*

1. First model: Beam with surface damping.

1.1. Formulation. Initially, only the most essential structural features are incorporated. Since some animals, notably the alligator and the anteater, have relatively straight cochleas, the coiled shape of the human cochlea is not considered essential for hearing [22]. A study stemming from this model includes the effects of coiling [63], [72]. Additionally, the basilar membrane in humans is quite narrow compared with its length (having average length, width and thickness of 30 mm, 2.5 mm and .01 mm respectively), and has considerable stiffness. Hence it is modeled as an uncoiled one-dimensional beam (Fig. 6), supported by hinges on both ends. Additionally, the rollers at the apical end indicate that small horizontal motions are not constrained. The motion of such a system is described by the one-dimensional beam equation

$$\frac{\partial^2}{\partial x^2}\left(EI\frac{\partial^2 Y(x,t)}{\partial x^2}\right) = -m\frac{\partial^2 Y(x,t)}{\partial t^2} + F(x,t). \tag{1}$$

As usual, E stands for the modulus of elasticity of the beam, I is the moment of inertia of the beam's cross-sectional area about the neutral axis, and m is the mass per unit length of the beam. The membrane oscillates in a viscous medium (the cochlear fluid) which produces the external forces $F(x,t)$. Happily, von Békésy has observed in

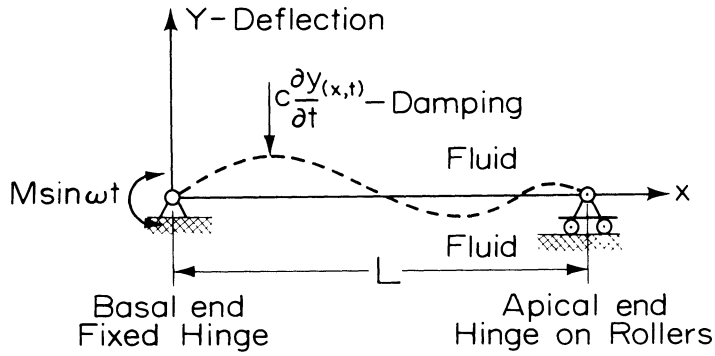

FIG. 6. *One-dimensional basilar membrane model.*

mechanical cochlear models, that the displacement patterns of the basilar membrane are fairly insensitive to drastic changes in the coupling between the membrane and the fluid [22]. A simplified coupling between the beam and fluid may, therefore, produce oscillatory characteristics similar to those of the actual basilar membrane. The displacements at the oval and round windows occur in opposite directions, very nearly out of phase in time [20]. Hence, for a single-frequency sound signal, the driving mechanism of the model can be approximated by a concentrated oscillating moment, $M \sin \omega t$, at the basal end (see boundary condition (4)). The fluid dampens the membrane's motion, and the damping force is assumed to be proportional to the vertical velocity of the membrane at each point, a satisfactory assumption for the low velocities encountered. In § 2, the damping term is rigorously derived.

Structurally, the membrane is assumed to be uniform in geometry, mass distribution and stiffness $(1/EI)$. The equation of motion for this model is

$$\frac{\partial^4 Y(x,t)}{\partial x^4} = -a^2 \frac{\partial^2 Y(x,t)}{\partial t^2} - b \frac{\partial Y(x,t)}{\partial t} \tag{2}$$

where $a^2 = m/(EI)$, $b = c/(EI)$, and c is proportional to the viscosity of the fluid. The negative sign is used for the damping force since this force always opposes motion, and its sign, therefore, is opposite to that of the vertical velocity.

The driving moment is introduced in the boundary conditions. For the basal end (fixed hinge) the vertical displacement is zero for all times,

$$Y(0,t) = 0, \qquad t \geqq 0, \tag{3}$$

and the bending moment is equal to the driving moment

$$EIY_{xx}(0,t) = -M \sin \omega t, \qquad t \geqq 0, \tag{4}$$

where the subscripts indicate partial differentiation. For the apical end (hinge on rollers) the boundary conditions are

$$Y(L,t) = Y_{xx}(L,t) = 0, \qquad t \geqq 0, \tag{5}$$

where L is the length of the membrane. The membrane is assumed to be initially at

:est; that is,

$$Y(x, 0) = Y_t(x, 0) = 0, \qquad 0 \leqq x \leqq L. \tag{6}$$

Equation (2), a linear partial differential equation with constant coefficients having the initial conditions (3), and subject to the boundary conditions (4) through (6), can be solved easily with the Laplace transformation. The details of the solution process may be found in [62].

The solution of (2) through (6) is

$$Y(x, t) = Y_{ST}(x, t) + Y_{TR}(x, t) \tag{7}$$

where

$$Y_{ST}(x, t) = A(x) \sin(\psi(x) + \omega t) \tag{8}$$

is the steady-state, and

$$Y_{TR}(x, t) = e^{-bt/2a^2} \sum_{n=1}^{\infty} \beta_n \sin(\alpha_n t + \theta_n) \sin n\pi x/L \tag{9}$$

is the transient part of the solution.

The specific forms of $A(x)$, $\psi(x)$, and the sine series in (9) are not important here. What is important is that the solution function obtained in (8) represents traveling wave motion (i.e., time dependent zeros or nodes), while (9) is the summation of decaying standing waves. For values of a and b roughly in the physiological range, the transients were computed and yielded standing waves. That is, both traveling waves and decaying standing waves are *simultaneously* present in the basilar membrane model. This result is of some interest. In physiological acoustics, some have theorized that the oscillations of the basilar membrane consist of standing waves, while a more widely accepted theory holds that only traveling waves are present. Depending on the value of the decay constant $b/(2a^2)$ for a short period after the introduction of the signal in the model, the standing waves dominate and obscure the behavior of the traveling waves. As the standing waves decay, the traveling waves become more prominent. Hence, the time elapsed after the basilar membrane is set in motion determines whether standing or traveling waves dominate. This observation offers a basis for reconciling the two seemingly conflicting theories.

The input signal in this model is of indefinite duration. Consequently, the presence of transients results from the initial rest condition of the membrane. For our purposes, the most important property of those transients is that, for all frequencies, they decay within half a millisecond and thus exhibit the known fast response of the basilar membrane.

1.2. Steady-state behavior and the place principle. A generally accepted modern version of the place principle exhibited by the motion of the basilar membrane holds that, though every tone spreads its effects throughout the cochlea, the high tones have oscillation patterns with maximum activity in the basal region, and the region of most vigorous action shifts toward the apical end as the frequency of the external signal decreases [20]. The solution functions of this model's steady-state behavior qualitatively reflect these observations.

It is natural to study the place principle by observing the time envelopes of the oscillations of the basilar membrane [22]. The time envelope of (8) is clearly the function $\pm A(x)$ which is known explicitly in terms of x, ω and the model parameters a and b. Figure 7 displays typical wave-form plots for one model configuration. The

position of the envelope maximum shifts toward the basal end of the membrane as the frequency of the signal increases. One quality of this model is immediately notable. Heretofore, the existence of a place principle has been attributed to the lengthwise variation of the stiffness of the basilar membrane due to its geometry. Yet, in this model, a place principle is markedly evident despite the uniform stiffness of the membrane.

If the place principle does not depend on the stiffness gradient of the basilar membrane, can the role of that gradient be illuminated by this model? Put another way, how would x_{max}, the position of the envelope's maximum, behave if the membrane had been modeled with a steep stiffness gradient along its length, with the basal end stiffest? Clearly, the deformation of the nonuniform membrane on the apical (i.e.,

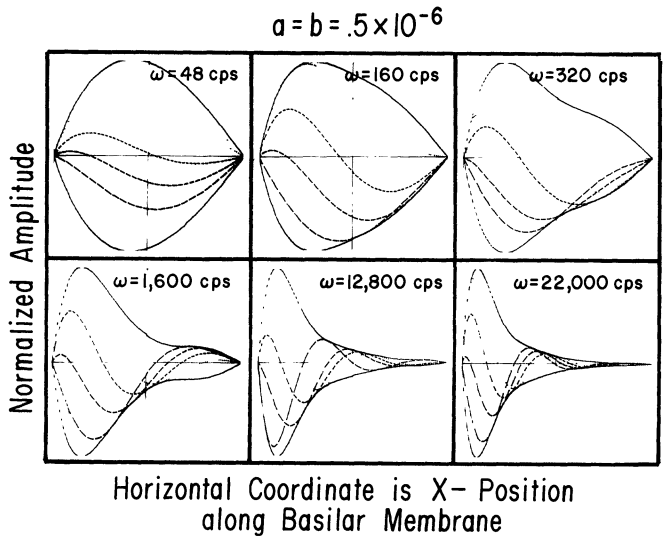

FIG. 7. *Time envelopes of basilar membrane's oscillations for first model, obtained on an IBM 2250 console.*

more pliant) side would be greater than that for a uniform membrane, while the deformation of the nonuniform membrane on the basal side would be less than that for a uniform membrane. Consequently, in the nonuniform membrane the envelope maxima occur farther to the right (toward the apical end) than in the uniform membrane. The shift in x_{max} will occur over a greater length of the membrane. The stiffness gradient, then, has the effect

$$\left(\frac{\Delta x_{max}}{\Delta \omega}\right)_n \geqq \left(\frac{\Delta x_{max}}{\Delta \omega}\right)_u \tag{10}$$

where the subscripts n and u stand for the nonuniform and uniform membranes respectively. The change in x_{max} is greater, and hence the change in frequency becomes more perceptible in a nonuniform basilar membrane. If the place principle accounts for frequency perception, the foregoing inequality indicates that the nonuniform membrane has a finer frequency discrimination than the uniform one.

Another aspect of the model is revealed by plotting x_{max} versus the input frequency ω (Fig. 8). The curves with a pronounced leftward shift in x_{max} for increasing ω correspond to the physiological range. The slopes of these curves become nearly vertical for large and small values of ω. This suggests the existence of auditory

"thresholds," with respect to frequency. Above and below certain frequencies, the shift in $x_{\max}$ for a change in ω is so small that it is not discernible. More precisely, there exists a range of a and b values such that

$$\lim_{\omega \to 0} (dx_{\max}/d\omega) = \lim_{\omega \to \infty} (dx_{\max}/d\omega) = 0. \tag{11}$$

Even drastic variations in the values of a and b produced the numerical result

$$x_{M0} = \lim_{\omega \to 0} x_{\max} \sim 12.73 \text{ mm} \tag{12}$$

for all values of a and b. It can be shown analytically that

$$x_{M0} \sim L(1 - 1/\sqrt{3}),$$

which, for $L = 30$ mm, confirms (12) independently of the value of a and b. This relationship provides the conjecture that the low frequency threshold of the membrane is a function of the geometry of the basilar membrane (in this case, the length L is the only geometrical property of the basilar membrane included in the model). The high frequency threshold, by contrast, is very sensitive to changes in a and b as is shown in Fig. 8. Since stiffness does not affect the low frequency threshold but does

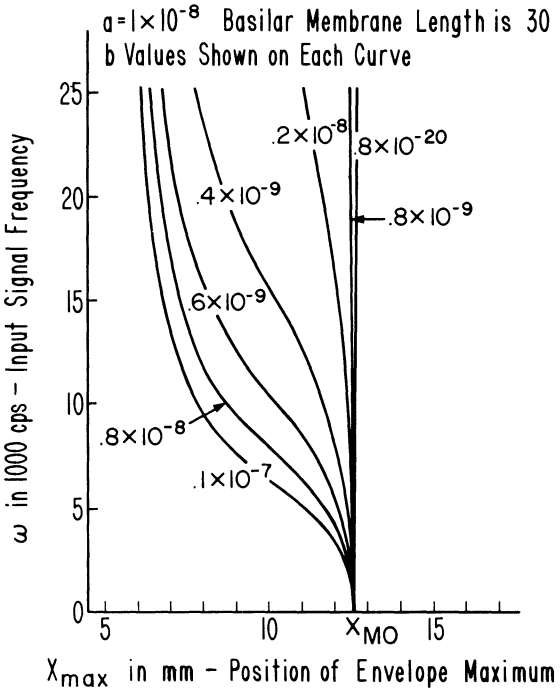

FIG. 8. *Place principle for first model.*

affect the high frequency threshold, changes in the stiffness of the basilar membrane that are likely to occur with aging will necessarily affect hearing only in the high frequency range. This is a plausible explanation for the phenomenon known as presbycusis in which only high frequency hearing diminishes with aging.

1.3. Reflections. Despite the simplicity of this two parameter model of the basilar membrane, it exhibits qualitative similarities to experimental evidence. It displays a

place principle, high and low auditory thresholds, and it suggests that the mechanisms responsible for the high frequency threshold are different from those responsible for the low frequency threshold. Qualitatively, it shows that the stiffness gradient of the basilar membrane is not responsible for the existence of the place principle, but is responsible for the fine frequency discrimination. Basilar membrane behavior at high frequencies is reasonably well represented, but the model's low frequency response is poor. Von Békésy's findings indicate that

$$\lim_{\omega \to 0} x_{\max} \sim L \text{ (length of the basilar membrane)},$$

while for this model

$$\lim_{\omega \to 0} x_{\max} \sim .42L.$$

This model, then, utilizes less than half of the basilar membrane's length for frequency discrimination. The third model, which incorporates the variable geometry of the cochlea, eliminates this deficiency and validates the conjecture that the low frequency behavior depends on cochlear geometry. A more accurate model requires a more complete treatment of both the fluid mechanics and cochlear geometry. In the second formulation, we superimpose a careful treatment of cochlear fluid dynamics on this model of the basilar membrane. The difference in the results of the two models will identify the effects of the coupling between the fluids and the basilar membrane on frequency discrimination and the auditory thresholds.

2. Second model: Beam in uniform cochlea.

2.1. Cochlear fluid mechanics. Because it is so thin, Reissner's membrane can transmit normal pressure from the scala vestibuli through the cochlear duct to the basilar membrane (see Fig. 3). However, any shear waves that may form on its upper surface as a consequence of its interaction with the fluid of the scala vestibuli will be attenuated by the contents of the cochlear duct before reaching the upper surface of the basilar membrane. Hence, Reissner's membrane and the jell-like fluid contents of the cochlear duct are represented by an idealized surface (capable of transmitting normal pressure, but not shear) contiguous to the upper surface of the basilar membrane. Further, it is assumed that no relative motion exists between the basilar membrane and this idealized surface. The new model is shown in Fig. 9, where, respectively, u, v, p and ρ denote the horizontal and vertical fluid velocities, pressure and density. The quantity $\nu = \mu/\rho$, where μ is the viscosity of the fluid, is the kinematic viscosity.

The general two-dimensional equations of motion for viscous and incompressible flows [90] are

$$u_x + v_y = 0, \tag{13}$$

$$u_t + uu_x + vu_y + \frac{1}{\rho} p_x = \nu(u_{xx} + u_{yy}), \tag{14}$$

$$v_t + uv_x + vv_y + \frac{1}{\rho} p_y = \nu(v_{xx} + v_{yy}), \tag{15}$$

wherein subscripts indicate partial derivatives.

Some observations on the motion of the system can be utilized to simplify (13), (14) and (15), and make them specific to our problem.

(i) The energy input occurs only in the x-direction through the piston-like movement of the stapes.

(ii) Due to the length scale difference $h \ll L$, the variations in the y-direction of the quantities defining the fluid field (i.e., p, v, u) will be relatively small.

(iii) We need to solve for the effect of the fluid on the basilar membrane surface (x, η) only, not at every point of the set $-h \leqq y \leqq h$ and $0 \geqq x \geqq L$.

(iv) The steady-state motion of the incompressible fluid, and the beam driven by it, will be periodic with period $T = 1/\omega$, where ω is the input frequency (as is the case in (8)). Viscous fluids form nearly stationary layers, called boundary layers, on the surfaces constraining their flow (e.g., the flow of honey on the sides of a jar). Such layers have a finite thickness, δ, within which the effects of viscosity are concentrated. We small make use of boundary layer theory (without detailing its intricacies) to note that for the boundary layer formed by such flows as ours [90, p. 354]

$$\delta \sim (\nu T)^{1/2} = (\nu/\omega)^{1/2}. \tag{16}$$

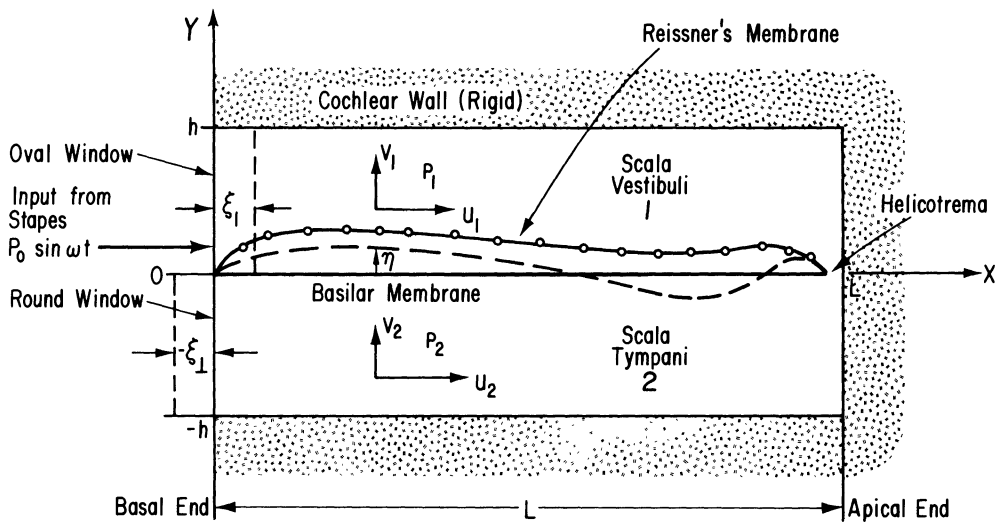

FIG. 9. *Two-dimensional cochlear model with uniform geometry.*

For $T \sim 10^{-2}$ sec (a very low frequency audio signal), and cochlear fluid kinematic viscosity $\nu \sim 1$ mm^2/sec [22], $\delta \sim 10^{-1}$ mm. The average height of the scalae tympani and vestibuli is approximately 1 mm, and the maximum basilar membrane displacement is less than 10^{-4} mm. Hence

$$\eta_{\max}/\delta \sim 10^{-3} \ll 1$$

(read the absolute value of the ratio of the maximum basilar membrane displacement to the thickness of the boundary layer is much less than 1). Consequently, the oscillations of the basilar membrane for all audio frequencies occur completely within the boundary layer.

Characteristically, in fluid dynamics, gross estimates of certain quantities are made to judge the relative importance of the terms appearing in the equations of motion of the fluid. We estimate the absolute values of

$$v \sim \frac{\eta_{\max}}{T}, \quad u_t \sim \frac{u}{T}, \quad v_y \sim \frac{\eta_{\max}}{T\delta},$$

since the main y-variations occur within the boundary layer. Then

$$\frac{uv_y}{u_t} \sim \frac{u\eta_{\max}/T\delta}{u/T} = \frac{\eta_{\max}}{\delta} \ll 1.$$

Further, from (13),

$$u_x = -v_y$$

which, together with the previous argument, shows that

$$uu_x/u_t \ll 1.$$

Hence, relative to the inertia term u_t, the nonlinear convective terms in (14) can be safely neglected.

Proceeding,

$$u_{xx} \sim \frac{u}{L^2} \quad \text{and} \quad u_{yy} \sim \frac{u}{\delta^2},$$

therefore

$$\frac{u_{xx}}{u_{yy}} \sim \left(\frac{\delta}{L}\right)^2 \ll 1$$

since $\delta \ll h \ll L$. Here we assume that $\lambda \ll h$, where λ is a "typical" wavelength of the basilar membrane's oscillations. Note, however, that

$$\frac{\nu u_{yy}}{u_t} \sim \frac{\nu T}{\delta^2} \sim 1,$$

which implies that νu_{yy} is the only viscous term that needs to be retained in (14).

We can now effectively eliminate the y-variation in u and p by defining averages. Let

$$\bar{u}_i(x, t) = \frac{(-1)^{i+1}}{h} \int_0^{(-1)^{i+1}h} u_i(x, y, t)\, dy, \qquad i = 1, 2, \tag{17}$$

where the subscripts 1 and 2 refer to the upper and lower chambers, respectively. The average pressure $\bar{p}_i(x, t)$ is defined similarly. As well, we have the boundary conditions

$$v_i(x, 0, t) = \eta_t, \qquad i = 1, 2, \tag{18}$$

which state that the vertical velocity of the fluid at the basilar membrane is exactly equal to the vertical velocity of the membrane, and

$$v_i(x, (-1)^{i+1}h, t) = 0, \qquad i = 1, 2, \tag{19}$$

which states that no fluid flows through the cochlear walls.

Applying (17), (18) and (19) to (13) and (14) (using the boundary layer no slip condition $\bar{u}_i(x, 0, t) = 0$ at the wall), and integrating, yields

$$\bar{u}_{ix} = \frac{(-1)^{i+1}}{h}\eta_t, \qquad i = 1, 2, \tag{20}$$

for the continuity equation, and

$$\bar{u}_{it} + \frac{1}{\rho} p_{ix} = \frac{\nu}{h} u_{iy}\Big|_0^{(-1)^{i+1}h} (-1)^{i+1}, \qquad i = 1, 2, \tag{21}$$

for the x-momentum. We shall see presently that (15), the y-momentum equation, is not needed to specify the motion of the basilar membrane.

Appealing again to classical boundary layer theory ([90], see also [76]) to obtain

$$\left.\frac{\partial u}{\partial y}\right|_{y=0} = \left(\frac{\omega}{4\nu}\right)^{1/2} \bar{u}(x, t),$$

we can simplify the right-hand term of (21) to

$$\bar{u}_{it} + \frac{1}{\rho} p_{ix} + r\bar{u}_i = 0 \tag{22}$$

where

$$r = \left(\frac{\omega\nu}{h^2}\right)^{1/2}.$$

A further redefinition of averages is advantageous. Letting

$$\begin{aligned} \bar{u} &= \tfrac{1}{2}(\bar{u}_1 - \bar{u}_2), \\ \bar{p} &= \tfrac{1}{2}(\bar{p}_1 - \bar{p}_2), \end{aligned} \tag{23}$$

results in the equations

$$u_x^- = 1/(h\eta_t), \tag{24}$$

$$u_t^- + 1/(\rho p_x^-) + ru^- = 0. \tag{25}$$

The equation of motion of the basilar membrane itself remains to be derived. Forces external to the membrane, resulting from the fluid acting on it, are shown in Fig. 10, where d is the thickness and m is the density of the membrane. The tangential

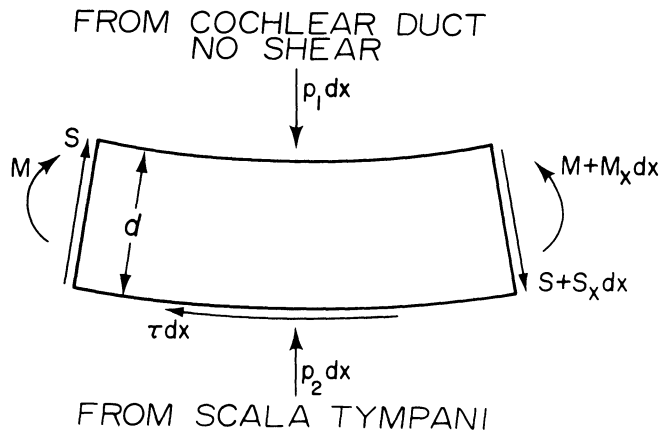

FIG. 10. *Forces on an element of the basilar membrane.*

force τ is the force acting on the beam as a result of the viscosity of the fluid. It results in a pointwise couple (torque) of size $\frac{1}{2}\, d\tau$ on the median of the beam. Using the equilibrium of the moments and vertical forces on the beam gives

$$EI\eta_{xxxx} + m\, d\eta_{tt} + 2p^- + \tfrac{1}{2}\, d\tau_x = 0.$$

Once again using (22), we obtain

$$\tau = \rho\nu u_{2y}(x, 0, t) = -\left(\frac{\nu\omega\rho^2}{4}\right)^{1/2} \bar{u}.$$

And via the averaged continuity equation (20), we obtain

$$\tau_x = \left(\frac{\nu\omega\rho^2}{4h^2}\right)^{1/2} \eta_t.$$

The final versions of the equations of motion in the system are the continuity equation (24), the x-momentum equation (25) and the beam equation

$$\eta_{xxxx} + \alpha^2\eta_{tt} + \gamma\eta_t + \beta p^- = 0 \tag{26}$$

where the coefficients are given by

$$\alpha^2 = md/(EI),$$

$$\beta = 2/(EI),$$

$$\gamma = \frac{d\rho}{4EIh}(\nu\omega)^{1/2}.$$

Note that (24), (25) and (26), together with appropriate initial and boundary conditions, suffice to describe the motion of the system, and that, as previously suggested, the y-variations are not important.[2] Note also that while the quantities u^- and p^- are averages, η (the deflection of the basilar membrane) is not. That is, no loss of information at the basilar membrane level occurs as a result of the averaging process.

The term $\gamma\eta_t$ in (26) is particularly interesting. It corresponds to the empirical damping term used in (2), the equation of motion for the first model. Here, however, the term reveals the physical nature of the damping—that is, the explicit dependence on the physical properties of the system and the input frequency.

2.2. Solution of the initial and boundary value problem. The equations of motion for the model are

$$\eta_{xxxx} + \alpha^2\eta_{tt} + \gamma\eta_t = -\beta p, \tag{26'}$$

$$u_x = \frac{1}{h}\eta_t, \tag{24'}$$

$$u_t = -\frac{1}{\rho}p_x - ru \tag{25'}$$

for $0 < x < L$ and $t > 0$.

For the sake of simplicity, the superscript $^-$ has been dropped with u and p denoting the averaged quantities, with negative superscript defined by (23).

The membrane and fluid are initially at rest; hence

$$\eta(x, 0) = \eta_t(x, 0) = 0,$$
$$u(x, 0) = 0 \tag{27}$$

for $0 \leqq x \leqq L$.

[2] Strictly speaking the net vertical load at the basilar membrane surface is

$$p_1(x, 0, t) - p_2(x, 0, t)$$

rather than the $2p^-$ appearing in (26). It is possible to show that $2p^-$ can be used as the vertical load, provided that the mass m and damping γ are altered to the virtual mass m_v and virtual damping γ_m. These can be estimated, but that would require a lengthy and unnecessary digression since no quantitative comparisons are intended and the actual values of m_v and γ_v are, therefore, not needed. The estimates, however, can be found in [74].

As in the first model the basilar membrane is assumed to be hinged at both ends resulting in the boundary conditions

$$\eta(0,t)=\eta(L,t)=0,\qquad \eta_{xx}(0,t)=\eta_{xx}(L,t)=0. \tag{28}$$

At the helicotrema (the orifice that connects the scalae vestibuli and tympani), where $x=L$, we assume that the pressures in the two chambers are equal and, consequently, result in zero average pressure so that

$$p(L,t)=0. \tag{29}$$

The whole system is driven by

$$p(0,t)=P_0\sin\omega t. \tag{30}$$

Conditions (28), (29) and (30) are valid for $t\geqq 0$.

According to Rhode's [82] measurements, there is a phase difference—dependent on the input frequency—between the motion of the tympanic membrane and the motion at the point where the incus and stapes are joined. For a simple harmonic input at the tympanic membrane, with frequency ω, we represent the input at the stapes by (30). The constant (for fixed ω) phase difference has been eliminated by a time translation. For more accurate representations of the middle ear function see Zwislocki [91], Møller [92] and the more recent work of Grant [93], Neiswander [94] and Whaley [95].

Three independent 6th order partial differential equations, one for each of the dependent variables, can be obtained from (26′), (24′) and (25′). The resulting equation for η involves only even derivatives with respect to x. Fortunately, the boundary conditions (28) also involve only even derivatives in x. Hence, η has a sine or cosine series expansion in x, since these functions repeat under double differentiation. Assuming that

$$\eta(x,t)=\sum_{n=1}^{\infty} f_n(t)\sin\frac{n\pi x}{L} \tag{31}$$

identically satisfies (28).

By direct substitution and via some obvious algebraic manipulation, the f_n are found to be

$$\begin{aligned} f_n(t)&=d^{-\lambda_n t}(c_{1n}\sin E_n t+c_{2n}\cos E_n t)\\ &\quad+d_{1n}\sin\omega t+d_{2n}\cos\omega t, \qquad n=1,2,\cdots, \end{aligned} \tag{32}$$

where

$$\begin{aligned} d_{1n}&=(-\omega^2A_n+C_n)D_n/\Delta_n, & d_{2n}&=-\omega B_nD_n/\Delta_n,\\ \Delta_n&=(-\omega^2A_n+C_n)^2+\omega^2B_n^2,\\ A_n&=\frac{L^2\rho}{n^2\pi^2h}+\frac{\alpha^2}{\beta}, & B_n&=\frac{L^2r\rho}{n^2\pi^2h}+\frac{\gamma}{\beta},\\ C_n&=\frac{n^4\pi^4}{L^4\beta}, & D_n&=-2P_0/n\pi,\\ E_n&=\sqrt{B_n^2-4A_nC_n}/2A_n, & \lambda_n&=B_n/2A_n, \end{aligned} \tag{33}$$

and

$$c_{1n}=-(\lambda_nd_{2n}+\omega d_{1n})/E_n, \qquad c_{2n}=-d_{2n}.$$

An easy application of the Weierstrass M-test shows that the convergence of the series is uniform for $0 \leqq x \leqq L$ and $t > 0$. In fact, the convergence is very rapid (d_{1n} as $1/n^5$ and d_{2n} as $1/n^9$). As before, an exact form for the time envelopes can be obtained.

In order to check the assumptions used in deriving the equations of motion, experiments were conducted with a mechanical facsimile of this cochlear model [36]. The observed displacement patterns of the model's basilar membrane closely resembled those described by (31).

2.3. What did we learn? In general, the results obtained from the second model (see [77] for detailed analysis) confirm and improve those obtained from the previous model. In this section we consider the possibility of resonance in the cochlea, and examine the time envelopes at high and low frequencies in order to determine the effects of the cochlear fluid on the place principle and auditory frequency thresholds.

2.3.1. Resonance. In this model, resonance can occur when the denominator Δ_n of d_{in}, $i = 1, 2$, is equal to zero. However, it is easy to see that there are no nonnegative zeros of the quartic polynomial Δ_n. The further possibility that resonance may occur when the denominator E_n of c_{in}, $i = 1, 2$, is equal to zero can also be ruled out easily. Hence, this model has no real and positive resonant frequencies. By contrast, Huxley [61] found that resonance can occur in a coiled cochlea.

2.3.2. Motion of the basilar membrane and the place principle. The oscillations of the basilar membrane model (31) can, again, be represented conveniently by

$$\eta(x, t) = \eta_{ST}(x, t) + \eta_{TR}(x, t), \tag{34}$$

where the subscripts ST and TR denote the steady-state and transient parts, respectively. In particular,

$$\eta_{ST}(x, t) = a_1(x) \sin \omega t + a_2(x) \cos \omega t \tag{35}$$

where

$$a_i(x) = \sum_{n=1}^{\infty} d_{in} \sin n\pi x/L, \qquad i = 1, 2. \tag{36}$$

More conveniently,

$$\eta_{ST}(x, t) = A(x) \sin (\omega t + \theta(x)) \tag{37}$$

where

$$\theta(x) = \sin^{-1} a_2(x)/A(x) = \cos^{-1} a_1(x)/A(x)$$

and

$$A(x) = [a_1^2(x) + a_2^2(x)]^{1/2}. \tag{38}$$

That is, $\eta_{ST}(x, t)$ consists of traveling waves having a maximum amplitude $A(x)$. The expression, $\eta_E(x)$, for the time envelopes of $\eta_{ST}(x, t)$ is simply

$$\eta_E(x) = \pm A(x).$$

It turns out that the transient portion makes no contribution to the time envelope of $\eta(x, t)$. Hence, we need study only the upper half, $A(x) \geqq 0$, of the envelopes (which are symmetrical with respect to the x axis) given by (38).

The place principle, for one model configuration, is shown in Fig. 11. Note that there exist secondary maxima towards the apical end. In Fig. 12 the effect of changes in E is illustrated. In curve 3 nearly vertical slopes occur for $2\text{ khz} < \omega < 7\text{ khz}$. Such regions of diminished sensitivity may explain some hearing disorders in selective frequency bands. In curve 4, the horizontal slope is an artifact caused by the growth of the secondary maxima until $\omega \sim 7$ khz where two equal relative maxima exist. Above and below this frequency there exist unique maxima.

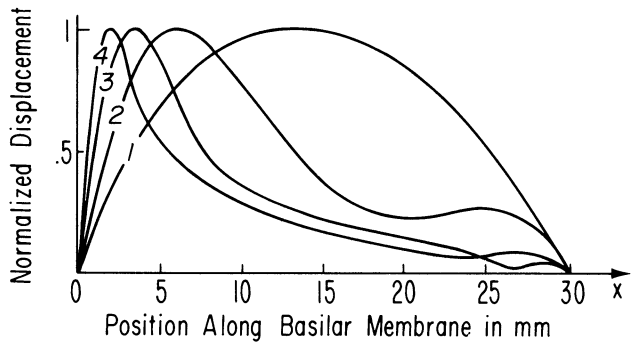

FIG. 11. *Time envelopes for second model. Curves correspond to the input frequencies in* hz (*cps*): # 1, 25 hz; # 2, 250; # 3, 2,500; # 4, 25,000.

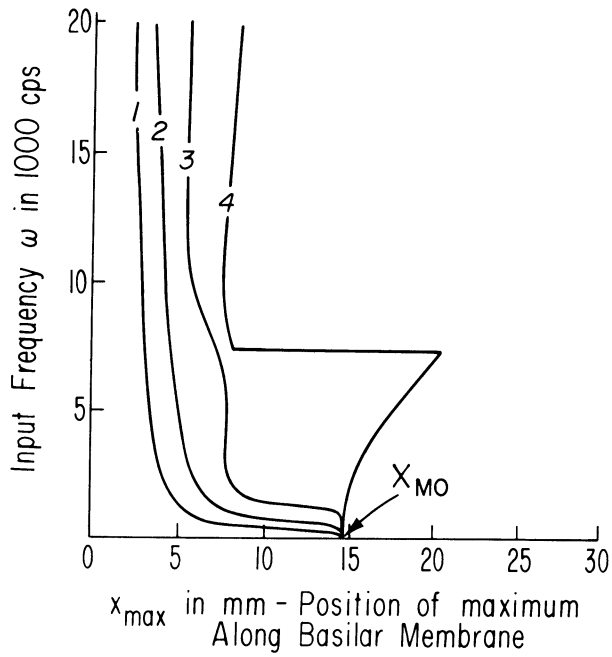

FIG. 12. *Place principle for second model. Curves correspond to different values of E in* N/m^2: # 1, 1.4×10^{13}; # 2, 1.4×10^{14}; # 3, 1.4×10^{15}; # 4, 1.4×10^{16}.

2.3.3. The place principle for high frequencies. As ω increases

$$d_{1n} \to -\frac{D_n}{A_n\omega^2} \quad \text{and} \quad d_{2n} \to -\frac{b_nD_n}{A_n^2\omega^{5/2}}$$

and $B_n = \omega^{1/2} b_n$.

For all ω the positions, x_E, of the extrema of the envelopes are given by

$$\frac{dA(x_E)}{dx} = 0 \tag{39}$$

which for large ω approaches

$$A_1(x_E)A_1'(x_E) + \frac{1}{\omega} A_2(x_E)A_2'(x_E) = 0, \tag{40}$$

where $a_1(x) = (1/\omega^2)A_1(x)$ and $a_2(x) = (1/\omega^{5/2})A_2(x)$ with $A_i(x)$, $i = 1, 2$, being independent of ω.

Differentiating with respect to ω yields

$$\frac{dx_E}{d\omega} = \frac{1}{\omega^2} \frac{A_2 A_2'}{A_\infty} \tag{41}$$

with

$$A_\infty = A_1 A_1'' + A_1'^2 + \frac{1}{\omega}(A_2 A_2'' + A_2'^2);$$

again for large ω,

$$AA'' + A'^2 = A_\infty.$$

If x_E is the position of a relative maximum (write $x_{\max}$), then

$$A''(x_{\max}) < 0,$$

so

$$A_\infty(x_{\max}) < 0. \tag{42}$$

Proceeding from (40) and (41),

$$\frac{dx_E}{d\omega} = -\frac{1}{\omega} \frac{A_1 A_1'}{A_\infty}. \tag{43}$$

The series $A_1(x)$ is easily summed:

$$A_1(x) = B \sum_{n=1}^{\infty} \frac{n}{n^2 + k^2} \sin \frac{n\pi x}{L} = B \sinh [\pi k(1 - x/L)] \tag{44}$$

where

$$B = -\frac{2P_0\beta}{\alpha^2 \pi} \quad \text{and} \quad k^2 = \frac{\beta L^2 \rho}{\alpha^2 \pi^2 h}. \tag{45}$$

For $0 \leqq x \leqq L$, then,

$$A_1(x)A_1'(x) < 0. \tag{46}$$

From (42), (43) and (44), we finally obtain

$$\frac{dx_{\max}}{d\omega} = -\frac{1}{\omega} \frac{A_1(x_{\max})A_1'(x_{\max})}{A_\infty(x_{\max})} < 0 \quad \text{for } \omega < \infty. \tag{47}$$

The point of this lengthy exercise is to deduce from (47) that

(i) $dx_{\max}/d\omega \to 0$ as $\omega \to \infty$.
(ii) $x_{\max} \downarrow \omega$ and in fact $x_{\max} \to 0$ as $\omega \to \infty$.

This is the place principle behavior at high frequencies.

As shown by (i), the sensitivity of the basilar membrane as a frequency analyzer diminishes as the frequency increases. Hence, past some frequency, frequency changes can no longer be detected. That is, there exists a high frequency "threshold" in the sense previously discussed.

The rate of change of $x_{\max}$ for large ω is given by (47), which incorporates the properties of the system (i.e., E, ρ, m, ν, h, d, and L), and thus establishes an explicit relationship between the high frequency threshold (sensitivity) and the physical properties of the model.

2.3.4. The place principle at low frequencies. As $\omega \to 0$, $A(x) \to |a_1(x)|$ with $d_{1n} = D_n/C_n$ since $d_{2n} \to 0$. The resulting sine series for the envelopes (and its sum) [96] is

$$\begin{aligned} A(x) &= c \sum_{n=1}^{\infty} (L^5/n^5)\pi^5 \sin n\pi x/L \\ &= (-c/240)u(u-1)(u^3 - 4u^2 - 8u/3 + 8/3) \end{aligned} \tag{48}$$

where $c = -2P_0\beta/L$, and $u = x/L$.

Equation (48) provides the shape of the envelopes as $\omega \to 0$ (which may be understood as a limit since at $\omega = 0$ the system is not in motion). The function given by (48) somewhat resembles the sine function for half a period (see low frequency envelope $\#1$ in Fig. 11), and its single maximum (to four significant figures) is $u = 0.4807$. Therefore,

$$x_{M0} = \lim_{\omega \to 0} x_{\max} = 0.4807L. \tag{49}$$

This confirms and improves the earlier result (equation (12)) that x_{M0} depends on the basilar membrane length.

We can appeal directly to the physics to obtain the same result. As $\omega \to 0$ the system approaches static equilibrium since no acceleration is imparted to the fluid and the basilar membrane (see also the discussion in § 3.2). By eliminating the time dependence in the dependent variables of the equations of motion, we obtain such conditions, and generate the uncoupled fluid equations

$$u_x = 0 \quad \text{and} \quad p_x = -\rho u \tag{50}$$

together with the beam equation

$$\eta_{xxxx} = -\beta p. \tag{51}$$

Appending the boundary condition (29) at the helicotrema, we find from (50) that

$$p(x) = \frac{\rho U}{L}\left[1 - \frac{x}{L}\right], \tag{52}$$

where U is the constant fluid velocity as $\omega \to 0$. Hence, in the limit $\omega \to 0$, the total load on the basilar membrane is the linearly distributed pressure given by (52). Inserting it in (51) gives for the deflection of the basilar membrane, the sum of the series in (48). So the "physical argument" is confirmed.

Some intriguing revelations emerge. The load, (52), is determined by the cochlea's geometry. Recall that, experimentally, $x_{M0} = L$. Further, $p(x)$ is monotone decreasing. Hence, the *only way* that $x_{M0} \sim L$ is for the basilar membrane to have a monotone decreasing stiffness (i.e., become increasingly pliant toward the apical end). The basilar membrane is isotropic (E = const.) and of constant thickness. Therefore, its monotone decreasing stiffness can be due only to its monotone increasing width (which increases $I(x)$ and decreases the stiffness, $1/EI(x)$). Ergo, the tapered shape of the real basilar membrane (that has a monotone increasing width toward the apical end) serves to increase the portion of its length active in frequency discrimination. This fact (discussed more fully in § 3) provides a glimpse into the intimate relationship between the system's geometry and low frequency hearing. Note, also, that for $\omega \to 0$, an analysis analogous to that for $\omega \to \infty$ establishes that

$$\lim_{\omega \to 0} dx_{\max}/d\omega = 0,$$

proving that even for a membrane with constant geometry, a low frequency threshold exists.

We have used the derivative $dx_{\max}/d\omega$ throughout as the criterion for the existence of auditory frequency thresholds because diminished sensitivity to *changes* in frequency (as indicated by $dx_{\max}/d\omega \to 0$) means that the ability to perceive tonal differentiation diminishes. However, rigorous criteria for frequency thresholds would also require that the maximum amplitude of basilar membrane oscillation at the threshold be very small. The amplitude condition for auditory frequency thresholds may be stated as follows; for k, a small nonnegative real number,

$$dx_{\max}/d\omega \to 0 \quad \text{and} \quad |\eta(x_{\max})| \leqq k \quad \text{as } \omega \to 0 \text{ or } \infty.$$

For high frequencies (see § 2.3.3), $x_{\max} \to 0$ and the amplitude decreases to zero due to the constraint at $x = 0$. At low frequencies, however, the maximum amplitude at the auditory frequency threshold is not small, since x_{M0}, in this model, is far from the constrained endpoint $x = L$.

2.4. Further reflections. The results from the first two models are substantially similar in that they both show excellent high-frequency but poor low-frequency response. The more rigorous second model yields more quantitative results. It demonstrates rather convincingly that while the effects of the cochlear fluids are most important at high frequencies, the effects of the variable geometry of the basilar membrane and the cochlea are required in the model to improve the low frequency response.

3. Third model: Tapered plate within oppositely tapered cochlea.

3.1. Cochlear geometry and low frequency behavior. The lower frequencies are most important, since they dominate in speech. (Telephones, for example, reliably transmit only up to approximately 2.5 khz.) The conclusions of § 2.3.4 show that in order to improve the model's low frequency response, it must be endowed with a variable geometry including the opposing tapers of the basilar membrane and the cochlea (as indicated in Fig. 13). The description of the geometry of the cochlea's main structures is, here, an idealization based on the data of Wever [18]. As in the previous models, the cochlea is modeled as an uncoiled body consisting of two rather than three chambers. The external shape of the uncoiled cochlea is well approximated by a conical surface of revolution. Internally, a plane consisting of the basilar membrane and its rigid supports divides the cochlea into two equal fluid-filled chambers (the

scalae tympani and vestibuli). Actually, the mid-plane is an idealized surface—called the cochlear partition—consisting of the basilar membrane with its supports and the collapsed cochlear duct including Reissner's membrane (see the discussion at the beginning of § 2.1). The width, $w(x)$, of the basilar membrane increases linearly as the cochlear cross section narrows. It is convenient to represent the basilar membrane as a circular sector of constant thickness, having a small opening angle α at the basal end (dotted lines in Fig. 13). Since the low-frequency effects are concentrated at the apical end, the small nonzero width of the basilar membrane at $x = 0$ can be safely neglected. As in the previous models, the system is driven by the piston-like movement of the stapes anchored at the oval window, and the fluid passes through the helicotrema connecting the two chambers.

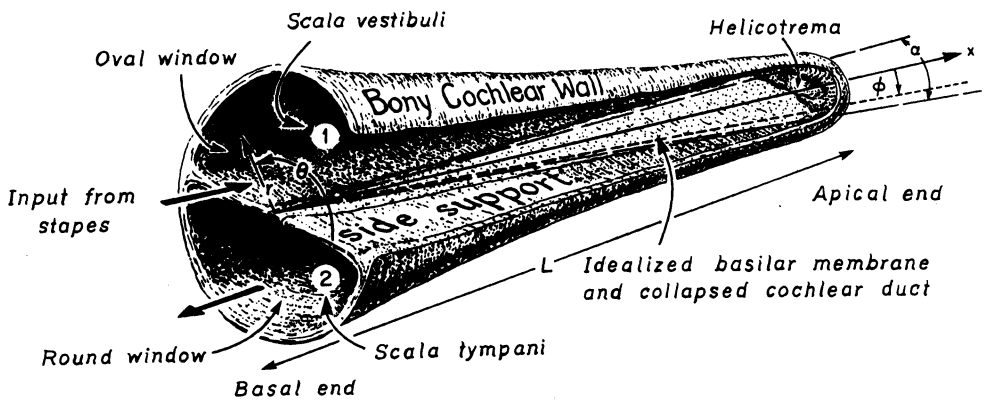

FIG. 13. *Three-dimensional two-chambered cochlear model.*

The mathematical description of the motion of such a system requires the 3-dimensional Navier–Stokes and continuity equations. The deflections of the 2-dimensional basilar membrane are described by the plate equation. Finding the simultaneous solutions of these partial differential equations for the appropriate initial and boundary conditions is, to put it mildly, a formidable task. However, as in § 2.1, a number of judicious simplifications can be used to make the problem tractable. Since we intend to study only the low frequency behavior of the model (as idealized by the limit $\omega \to 0$), numerous terms can be excluded from the equations of motion.

In outline form (see [80] for details), the formulation proceeds as follows.

A number of small terms in the equations of motion of the fluid can be neglected, and the net averages

$$p(x,t) = \tfrac{1}{2}(\bar{p}_1 - \bar{p}_2), \quad u(x,t) = \tfrac{1}{2}(\bar{u}_1 - \bar{u}_2)$$

may be defined, where $\bar{p}_i$ and $\bar{u}_i$ are the averaged (now over the cross sectional area) pressure and velocity in the x-direction, and $i = 1, 2$ is the index specifying the chamber.

This yields

$$\frac{\partial}{\partial x}[A(x)u(x,t)] = w(x)\bar{\eta}_t(x,t) \tag{53}$$

for the continuity equation, where $\bar{\eta}$ is the averaged (over φ) deflection of the basilar membrane, and $A(x)$ is the cross sectional area of each chamber. Note that for

cochlear chambers having constant rectangular cross section of height h and the same width w as the basilar membrane, (53) reduces as it should, to (24).

The averaged x-momentum equation is

$$u_t + \frac{1}{\rho} p_x + \left(\frac{\nu\omega}{2}\right)^{1/2} \frac{C(x)}{A(x)} u = 0, \tag{54}$$

where, as before, ρ and ν are the density and kinematic viscosity of the fluid and ω is the frequency of the input signal. The circumference of each chamber (including the portion along the mid-plane) is denoted by $C(x)$. The ratio $C(x)/A(x)$ is, of course, characteristic of the geometry. For our semi-circular cross section,

$$\left(\frac{\nu\omega}{2}\right)^{1/2} \frac{C(x)}{A(x)} = \frac{(2\omega\nu)^{1/2}}{r}\left(\frac{1}{2} + \frac{1}{\pi}\right) = \frac{K(\omega)}{r},$$

which differs only slightly in the constant factor from the equivalent coefficient in (25).

The deformation, η, of a circular sector with constant thickness d (the basilar membrane in this model), is given by (see (191) in [97])

$$\left(D\Delta^2 + m(x)\frac{\partial^2}{\partial t^2} + c(x)\frac{\partial}{\partial t}\right)\eta(x, \varphi, t) = p_{\text{net}}(x, \varphi, t), \tag{55}$$

where $D = Ed^3/[12(1 - N^2)]$, N is the Poisson ratio of the plate's material, and

$$\Delta = \frac{\partial^2}{\partial x^2} + \frac{1}{x}\frac{\partial}{\partial x} + \frac{1}{x^2}\frac{\partial^2}{\partial \varphi^2}$$

is the Laplacian operator in the plane of the basilar membrane. The mass, $m(x)$, and damping, $c(x)$, of the basilar membrane here are x dependent due to the variable geometry of the model. The term $p_{\text{net}}(x, \varphi, t)$ denotes the net pressure (difference between pressures) at the surface ($\theta = 0$ or $\theta = \pi$) of the basilar membrane. By convention, downward pointing net pressure ($\theta = -\pi/2$) is positive. The formal similarity of (55) to (26) is evident. Note that in contrast to (53) the deflection η (rather than an averaged deflection) appears in (55).

Along the edges, $\varphi = \pm\alpha/2$, the basilar membrane merges with the bony cochlear walls and is assumed to be supported by fixed hinges (in the parlance of elasticity theory this condition is often referred to as simply supported), yielding the boundary conditions (see [97, (193i)])

$$\begin{cases} 0 \leqq x < L \quad \text{and} \quad t \geqq 0, \\ \eta\left(x, \pm\dfrac{\alpha}{2}, t\right) = 0, \\ \eta_{xx}\left(x, \pm\dfrac{\alpha}{2}, t\right) + N\left[\dfrac{1}{x}\eta_x\left(x, \pm\dfrac{\alpha}{2}, t\right) + \dfrac{1}{x^2}\eta_{\varphi\varphi}\left(x, \pm\dfrac{\alpha}{2}, t\right)\right] = 0. \end{cases} \tag{56}$$

The second condition states that the hinges at $\varphi = \pm\alpha/2$ provide no resisting moment (see (5) to appreciate the added complexity due to the plate). Note also that (56) includes the point at the origin $x = 0$. Specifying the boundary conditions at $x = L$ requires considerable care and these conditions will be discussed in the next section.

Derivatives with respect to φ appear only in (55) and in the boundary condition (56). In both cases they are even derivatives and this implies that η can be expanded into a sine or cosine series in φ (linear combinations of sine and cosine functions are closed with respect to even differentiation). The cosine series is more convenient and

in fact the odd-indexed terms suffice. We take

$$\eta(x, \varphi, t) = \sum_{n=0}^{\infty} a_n(x, t) \cos(2n+1)m\varphi, \quad \text{where } m = \frac{\pi}{\alpha} \sim 400, \tag{57}$$

which directly satisfies the boundary conditions (56). The terms of this trigonometric series represent the various transverse (across φ) modes of vibration of a sectorial plate simply supported along its radial edges. We argue, heuristically, that the plate is extremely narrow (α is small) and the energy input is too low to excite the higher modes (i.e., multiple nodes across φ). We seek then only the lowest (i.e., fundamental) mode[3] for η:

$$\eta(x, \varphi, t) = a_0(x, t) \cos m\varphi. \tag{58}$$

The maximum η, due to symmetry, will occur along the center line $\varphi = 0$. To study the place principle then, it suffices to know the centerline deflection

$$\eta(x, 0, t) = a_0(x, t).$$

From (58) and (55) we deduce

$$\left(DE_x^4 + m(x)\frac{\partial^2}{\partial t^2} + c(x)\frac{\partial}{\partial t}\right) a_0(x, t) \cos m\varphi = p_{\text{net}}(x, \varphi, t) \tag{59}$$

where

$$E_x^4 = \left(\frac{\partial^2}{\partial x^2} + \frac{1}{x}\frac{\partial}{\partial x} - \frac{m^2}{x^2}\right)^2$$

is a fourth-order differential operator in x of the Euler type. Equation (59), being valid at every point of the basilar membrane, is also true for the centerline $\varphi = 0$, hence

$$\left(DE_x^4 + m(x)\frac{\partial^2}{\partial t^2} + c(x)\frac{\partial}{\partial t}\right) a_0(x, t) = p_{\text{net}}(x, 0, t). \tag{60}$$

The x-momentum, (54), is expressed in terms of the averaged pressure p, rather than the net pressure p_{net} appearing in (60). To connect these two equations, we replace p_{net} by $2p$. As discussed in footnote 2, this can be done provided that $m(x)$ and $c(x)$ are replaced by $m_v(x)$ and $c_v(x)$, the *virtual* mass and damping, resulting in

$$\left(DE_x^4 + m_v(x)\frac{\partial^2}{\partial t^2} + c_v(x)\frac{\partial}{\partial t}\right) a_0(x, t) = 2p(x, t). \tag{61}$$

It will be seen in § 3.2 that the specific forms of m_v and c_v are not needed for the limiting case $\omega \to 0$.

To complete the formulation we compute $\bar{\eta}$, arising in (53), by

$$\bar{\eta}(x, t) = \frac{1}{w(x)} \int_{-\alpha/2}^{\alpha/2} \eta(x, \varphi, t)\, d\varphi,$$

where $w(x)\bar{\eta}(x, t)$ is the instantaneous area, at x, swept-out between the mid-plane and the deflected basilar membrane. This yields for (53),

$$\frac{\partial}{\partial x}[A(x)u(x, t)] = \frac{2}{m}\frac{\partial}{\partial t} a_0(x, t). \tag{62}$$

[3] In (53), the φ variation of η has been averaged. To find the higher modes, the equations need to be reformulated with all the variables containing their variation in φ.

Equations (54), (61) and (62) describe the centerline deflection $a_0(x, t)$ in terms of the averaged quantities $u(x, t)$ and $p(x, t)$. Notice that spatially the equations are one-dimensional as in the previous two models.

3.2. Solution of the equations of motion as $\omega \to 0$. We noted previously (see the end of § 2.3.4) that as $\omega \to 0$ the system approaches static equilibrium (i.e., the fluid and basilar membrane do not accelerate). The Reynolds number, for our system, may be estimated by

$$\mathrm{Re} = \frac{\rho \xi \omega L}{\mu}$$

where ξ is a "typical" displacement of the oval window in the x-direction. In the jargon of fluid mechanics, the limit $\omega \to 0$ results in Stokes' (or "creeping") flow. Such flows occur elsewhere in biofluidmechanics (e.g., see [98]). In our case this condition is described by the equations of motion when the time-dependence is eliminated, yielding

$$\frac{d}{dx}[A(x)u_0] = 0 \tag{63}$$

and

$$\frac{1}{\rho}\frac{dp_0}{dx} + \frac{K(\omega)}{r}u_0 = 0 \tag{64}$$

for the now uncoupled fluid equations, and

$$E_x^4 a_0 = \frac{2}{D} p_0 = I(x) \tag{65}$$

for the deflection of the basilar membrane's centerline. The subscript 0 denotes the limiting values of the variables as $\omega \to 0$.

3.2.1. Load on the basilar membrane. We deduce from (63) that $u_0 = k_1/A(x)$ with k_1 a constant of integration, enabling us to integrate (64) and find, when $A(x) = \pi r^2(x)/2$, that

$$p_0 = \beta G(x) + k_2$$

with

$$\beta = -\frac{2\rho k_1 K(\omega)}{\pi}, \qquad G(x) = \int_0^x \frac{ds}{r^3(s)}$$

and k_2 being the second integration constant. The constants k_1 and k_2 are determined from the boundary conditions

$$p_0(0) = S_0 \quad \text{the input pressure} \tag{66a}$$

and

$$p_0(L) = PS_0, \quad 0 \leqq P < 1, \quad \text{the pressure difference.} \tag{66b}$$

The last condition differs from the equivalent condition of the previous model where the pressure was equalized at the helicotrema ($p(L, t) = 0$). Here we allow for a

nonzero pressure difference at $x = L$, for reasons which are discussed in § 3.3. We find that

$$p_0(x) = S_0\left[1-(1-P)\frac{G(x)}{G(L)}\right]. \tag{67}$$

This remarkable formula gives the load, $p_0(x)$, on the basilar membrane for an *arbitrary* cochlear radius $r(x) \neq 0$ (i.e., for any cochlea whose boundary is a surface of revolution). Its striking simplicity belies its importance.

As an example, for the model in § 2 where $r(x) = h$ a constant, $G(x) = x/h^3$. Trivially, then, for $P = 0$,

$$p_0(x) = S_0\left(1-\frac{x}{L}\right),$$

gives the linearly distributed load (equation (52)), which we previously found the hard way.

The tacit assumption is that $r(x) \neq 0$, $\forall x \in [0, L]$, for otherwise the cochlea would be blocked. To assure that $1/r^3(x)$ is Riemann integrable on $[0, L]$ it suffices to take $r(x)$ continuous there. Actually, continuity of $r(x)$ additionally implies the existence and continuity of $G'(x) = 1/r^3(x)$ on $(0, L)$.

We note that $G(x) \geqq 0$ and is strictly monotone increasing since $r(x) > 0$. This, in turn, implies that $p_0(x)$ is strictly monotone decreasing and bounded by $PS_0 \leqq p_0(x) \leqq S_0$.

It is instructive to invert (67), where

$$p_0'(x) = \frac{k}{r^3(x)}$$

with

$$k = -\frac{S_0(1-p)}{G(L)} \quad \text{a constant.}$$

We deduce that

$$r(x) = \left(\frac{k}{p_0'(x)}\right)^{1/3} \quad \text{positive root.} \tag{68}$$

For $k < 0$ and $p_0'(x) < 0$, (68) always has a unique real and positive root.

By specifying an additional side condition, such as

$$r(0) = r_0, \tag{69}$$

and a desired pressure difference, $p_0(x)$, on the basilar membrane as $\omega \to 0$ (with $p_0'(x) < 0$), equations (68) and (69) yield the *unique* cochlear geometry responsible for such a load.

For example, let us take the linearly distributed pressure difference obtained from a uniform cochlea. Then

$$p_0'(x) = -\frac{S_0}{L} < 0$$

and

$$r(x) = \left(-\frac{kL}{S_0}\right)^{1/3} = r_0 \quad \text{a constant.}$$

Hence, we can either "control" the load, via (67), by specifying the cochlear geometry by $r(x)$, or conversely via (68) and (69).

3.2.2. Deflection of the basilar membrane's centerline. Having the load we can invoke

$$E_x^4 a_0 = I(x) \tag{65}$$

to find the resulting centerline deflection.

For boundary conditions we have at the origin

$$a_0(0) = 0, \tag{70}$$

a condition which stems from the first part of (59). At the apical end, where $x = L$, the situation is quite complex, and three kinds of end supports—hinged end, free end, and elastic end—are investigated in the next section. The need for this complexity is discussed in § 3.3. All these constraints are expressed as particular cases (specifying the c_{ij}) of the two independent linear combinations:

$$\begin{cases} c_{11}a_0(1) + c_{12}a_0'(1) + c_{13}a_0''(1) + c_{14}a_0'''(1) = 0, \\ c_{21}a_0(1) + c_{22}a_0'(1) + c_{23}a_0''(1) + c_{24}a_0'''(1) = 0, \end{cases} \tag{71}$$

where the normalization $x \to x/L$ is conveniently used from now on.

The complementary solution of (65) is

$$a_{0_c}(x) = Ax^m + Bx^{-m} + Cx^{m+2} + Dx^{-(m+2)}. \tag{72}$$

From (70) it is seen that $B = D = 0$ so that the two conditions in (71) suffice to determine the remaining two constants.

To find a particular solution we use the time honored method of LaGrange assuming that

$$a_{0_p}(x) = A(x)x^m + C(x)x^{m+2}. \tag{73}$$

The unknown functions $A(x)$ and $C(x)$ are determined from (65). This, however, yields only one condition where two are needed. We assume the additional consistent condition

$$C''x^3 + (2m+5)C'x^2 + A''x + (2m+1)A' = 0. \tag{74}$$

Equations (65), (73) and (74) jointly imply that

$$C''x + (2m+1)C' = \frac{I(x)}{4(m+1)x^{m-1}} = R(x). \tag{75}$$

We reduce the order of (78) by

$$C' = q(x) \tag{76}$$

yielding the first order equation

$$xq' + (2m+1)q = R(x)$$

whose solution is

$$q(x) = \frac{1}{x^{2m+1}} \int_z^x x_1^{2m} R(x_1)\, dx_1.$$

Here z is an arbitrary constant. Since a particular solution is sought no arbitrary constants are required and any convenient value for z will do. Typically, the simplest particular solution is given when z is a zero, if one exists, of the integrated function (anti-derivative). This comment also applies to the lower limits z_i, $i = 1, \cdots, 4$, in the subsequent integrals. Integrating again, we get

$$C(x) = \int_{z_1}^{x} \frac{1}{x_2^{2m+1}} \left\{ \int_{z_2}^{x_2} x_1^{2m} R(x_1)\, dx_1 \right\} dx_2. \tag{77}$$

From (77) and (74) we have

$$A''x + (2m+1)A' = -x^2 R - \frac{4}{x^{2m-1}} \int_{z_2}^{x} x_1^{2m} R(x_1)\, dx_1 = H(x),$$

an equation identical to (75) with A and H instead of C and R (!). Hence,

$$A(x) = \int_{z_4}^{x} \frac{1}{x_4^{2m+1}} \left\{ \int_{z_3}^{x_4} x_3^{2m} H(x_3)\, dx_3 \right\} dx_4. \tag{78}$$

Altogether then

$$a_0(x) = (A + A(x))x^m + (C + C(x))x^{m+2} \tag{79}$$

provides the centerline deflection due to the load induced by the cochlear geometry. With A and C determined from the boundary conditions, (70) and (82) determine the response as $\omega \to 0$ as a function of the geometry and boundary conditions of the system. The position, $x_{\max}$, of the maximum deflection is independent of the membrane's elastic properties, since the basilar membrane is assumed to be isotropic (E and N constant).

3.2.3. Boundary conditions at the helicotrema. For reasons best discussed later, three sets of boundary conditions for the basilar membrane's apical end ($x = 1$ in the normalized coordinate) are considered. It is convenient to write the deflection as

$$a_0(x) = Ax^m + Cx^{m+2} + a_{0_p}(x) \tag{80}$$

since $a_{0_p}(x)$ is independent of the constraints.

In the previous models the boundary conditions everywhere (i.e., the two endpoints) were simple supports (hinges). For the sake of comparison we impose, at first, simple supports at all the boundaries of the sectorial plate. Recall that we already have the long edges, $\varphi = \pm\alpha/2$, including the origin simply supported (condition (56)). For $x = 1$ we have then

$$\begin{cases} \eta(1, \varphi, t) = 0, \\ \eta_{xx}(1, \varphi, t) + N\left[\frac{1}{x}\eta_x(1, \varphi, t) + \frac{1}{x^2}\eta_{\varphi\varphi}(1, \varphi, t)\right] = 0, \end{cases} \tag{81}$$

which for the centerline $\varphi = 0$, and the form (58) with the time variable eliminated reduces to

$$\begin{cases} a_0(1) = 0, \\ a_0''(1) + N a_0'(1) = 0. \end{cases} \tag{82}$$

Substituting (80) and solving yields

$$A_H = \frac{-(m+2)(m+1+N)a_{0_p}(1) + Na'_{0_p}(1) + a''_{0_p}(1)}{2(2m+1+N)} \tag{83}$$

and

$$C_H = \frac{m(m-1+N)a_{0_p}(1) - Na'_{0_p}(1) - a''_{0_p}(1)}{2(2m+1+N)} \tag{84}$$

for the two constants with the subscript H indicating the hinged-end condition.

The next condition investigated is the free-end, where as the name implies the end is unconstrained. In polar coordinates[4] this condition is expressed by

$$\eta_{xx} + N\left(\frac{1}{x}\eta_x + \frac{1}{x^2}\eta_{\varphi\varphi}\right)\Big|_{\substack{\varphi=0\\x=1}} = 0$$

indicating no resisting moment[5] and

$$\eta_{xxx} + (2-N)\left\{\frac{1}{x}\eta_{xx} - \frac{1}{x^2}\eta_x + \frac{1}{x^2}\eta_{x\varphi\varphi} - \frac{2}{x^3}\eta_{\varphi\varphi}\right\}\Big|_{\substack{\varphi=0\\x=1}} = 0,$$

indicating no resisting shear at $x = 1$.

Again via (58) these reduce to

$$a''_0(1) + N(a'_0(1) - m^2 a_0(1)) = 0 \tag{85a}$$

and

$$a'''_0(1) + (2-N)(a''_0(1) - (1+m^2)a'_0(1) + 2m^2 a_0(1)) = 0. \tag{85b}$$

Indicating the coefficients for the free-end condictions by the subscript F we obtain, after some rather laborious algebra,

$$A_F = \frac{E_F(m+2N_F) - e_F m(m+2M_F)}{2m(m-1)(m-2P_F)(3+N)} \tag{86}$$

and

$$C_F = \frac{e_F(m-2) - E_F}{2(m+1)(m-2P_F)(3+N)}, \tag{87}$$

where

$$N_F = \frac{1+N}{1-N}, \quad M_F = -\frac{3-N}{1-N}, \quad P_F = \frac{1+N}{3+N},$$

$$E_F = a'''_{0_p}(1) + (2-N)\{a''_{0_p}(1) - (1+m^2)a'_{0_p}(1) + 2m^2 a_{0_p}(1)\},$$

and

$$e_F = -a''_{0_p}(1) - Na'_{0_p}(1) + Nm^2 a_{0_p}(1).$$

[4] The equations given by Timoshenko [97, p. 284] are incorrect. The correct expressions used here were obtained from Timoshenko's conditions in Cartesian coordinates [97, p. 84] transformed directly to polar coordinates.

[5] The notation $|_{\substack{\varphi=0\\x=1}}$ means that the whole expression is evaluated at $\varphi = 0$ and $x = 1$.

In the language of elasticity theory, the fine structure of the basilar membrane at the helicotrema is well described by a condition called an elastic-end. A narrow beam at the end functions as a ligament constraining both the rotation and translation of the basilar membrane there.

Transforming Timoshenko's [97, p. 86] elastic end conditions at $x = 1$ to polar coordinates we obtain

$$D\{\eta_{xx} + N(\eta_x + \eta_{\varphi\varphi})\}\Big|_{\substack{x=1\\ \varphi=0}} = -C(\eta_{xx} + \eta_{x\varphi\varphi} - \eta_x - 2\eta_{\varphi\varphi})\Big|_{\substack{x=1\\ \varphi=0}} \tag{88}$$

for rotational equilibrium, where C is the torsional rigidity[6] of the end beam. The left-hand side of (88) represents the twisting moment at the end ($x = 1$) of the basilar membrane, which is balanced by the resisting twisting moment of the ligament (end beam). Translational equilibrium yields

$$\begin{aligned} &D\{\eta_{xxx} + (2-N)[\eta_{xx} + \eta_{x\varphi\varphi} - \eta_x - 2\eta_{\varphi\varphi}]\}\Big|_{\substack{x=1\\ \varphi=0}} \\ &\qquad = B(3\eta_{xx} + 6\eta_{x\varphi\varphi} - 3\eta_x - 8\eta_{\varphi\varphi} + \eta_{\varphi\varphi\varphi\varphi})\Big|_{\substack{x=1\\ \varphi=0}}, \end{aligned} \tag{89}$$

where B is the flexural rigidity of the end beam. It stems from the equal deflections of the basilar membrane and end beam along $x = 1$.

From (58) the elastic-end conditions reduce to

$$(1-a)a_0''(1) + [(m^2+1)a + N]a_0'(1) - m^2(N+2a)a_0(1) = 0 \tag{90}$$

and

$$\begin{aligned} &a_0'''(1) + (2-N-3b)a_0''(1) + [-(2-N)(m^2+1) + 3b(2m^2+1)]a_0'(1) \\ &\qquad + [2m^2(2-N) - m^2b(8+m^2)]a_0(1) = 0, \end{aligned} \tag{91}$$

where $a = -C/D$ and $b = B/D$.

When $a = b = 0$ the end beam offers no constraints and (88) and (89) reduce to the free-end as a special case.

Solving for the constraints in (80), from (90) and (91), a painstaking task, and subscripting by E, results in

$$A_E = \frac{e_E m(m + 2M_E) - E_E(m + 2N_E)}{m(m-1)(1-N)Q} \tag{92}$$

and

$$C_E = \frac{E_E - e_E(m-2)}{m(m+1)(1-N)Q} \tag{93}$$

[6] This quantity, for torsional loads (moments) plays the same role as EI—the flexural rigidity—plays for transverse loads.

with

$$Q = m(m+2M_E) - (m-2)(m+2N_E),$$

$$T = 1 + \frac{a(m-2)}{1-N}, \quad N_E = \frac{1+N}{T(1-N)}, \quad P_E = 1 + \frac{b(m-3)}{1-N},$$

$$M_E = \frac{N-3-b(2m-3)}{1-N+b(m-3)}, \quad E_E = \frac{E_{E_1}}{P_E}, \quad e_E = \frac{e_{E_1}}{T},$$

$$e_{E_1} = -(1-a)a''_{0_p}(1) - [(m^2+1)a+N]a'_{0_p}(1) + m^2(N+2a)a_{0_p}(1)$$

and

$$E_{E_1} = a'''_{0_p}(1) + [(2-N)-3b]a''_{0_p}(1) + [-(2-N)(m^2+1) + 3b(2m^2+1)]a'_{0_p}(1) + [2m^2(2-N) - m^2b(8+m^2)]a_{0_p}(1).$$

We can now study the behavior of the model as $\omega \to 0$.

3.3. The contributions of the cochlea's geometry. Equation (67) succinctly unbares the reasons for the cochlea's curious geometry. It implies that *any* symmetric cochlea induces a strictly monotone decreasing load, $p_0(x)$ as $\omega \to 0$, on the basilar membrane. Recall that, due to the input at $x = 0$, $\lim_{\omega\to\infty} x_{\max} = 0$ and further that $x_{\max} \downarrow \omega$ (place principle). To optimize, that is use the full length of the basilar membrane for frequency discrimination, nature put x_{M0} at $x = 1$. Only if *the basilar membrane has a monotone decreasing stiffness matching the monotone decreasing load* $p_0(x)$ can x_{M0} be close to $x = 1$. This explains the widening taper of the real basilar membrane, and is the key to understanding the cochlea's geometry. The "rest" falls into place as the story unfolds.

In the ensuing computations we have set $m = 400$. The value of the Poisson ratio, N ($0 \leqq N \leqq 1$ for all materials) of the basilar membrane is not known. Fortunately, the basilar membrane's centerline (BMC) deflection $a_0(x)$, is insensitive to drastic variations in the value of N and m. For $0.2 \leqq N \leqq 0.7$ and $100 \leqq m \leqq 600$ the computed variation of x_{M0} is less than 1%.

The BMC deflection $a_0(x)$ resulting from the linearly distributed load induced by a uniform ($r(x) = \text{const.}$) cochlea is shown in Fig. 14. For all end conditions at the helicotrema $x_{M0} = .80$, a considerable improvement from the previous $x_{M0} = .48$ though still far from $x = 1$. Since the decreasing stiffness of the tapered basilar membrane does not alone suffice to place x_{M0} close to 1, we superimpose the narrowing of the cochlea.

In evaluating the load, $p_0(x)$, it is convenient to consider "hyperbolic cochleas" of the form

$$r(x) = \frac{c}{(x+d)^p} \quad \text{for } p > 0. \tag{94}$$

A natural way to determine d is by specifying the ratio $R = r(0)/r(1)$ which measures the cochlea's narrowing ("taper"). The constant c is superfluous for it is canceled out in (67). In humans $R \sim 3$ and in the range $\frac{1}{3} \leqq p \leqq 2$, equation (94) yields shapes resembling that of an uncoiled cochlea.

For $p = 1$ and various R the induced loads are displayed in Fig. 15. For $R > 1$ (narrowing cochleas), the induced load is greater pointwise than the linear load due to a uniform cochlea, while for $R < 1$ (widening cochlea) the load is smaller pointwise. Clearly, the cochlea's narrowing helps by shifting (farther than .80) x_{M0} to the right.

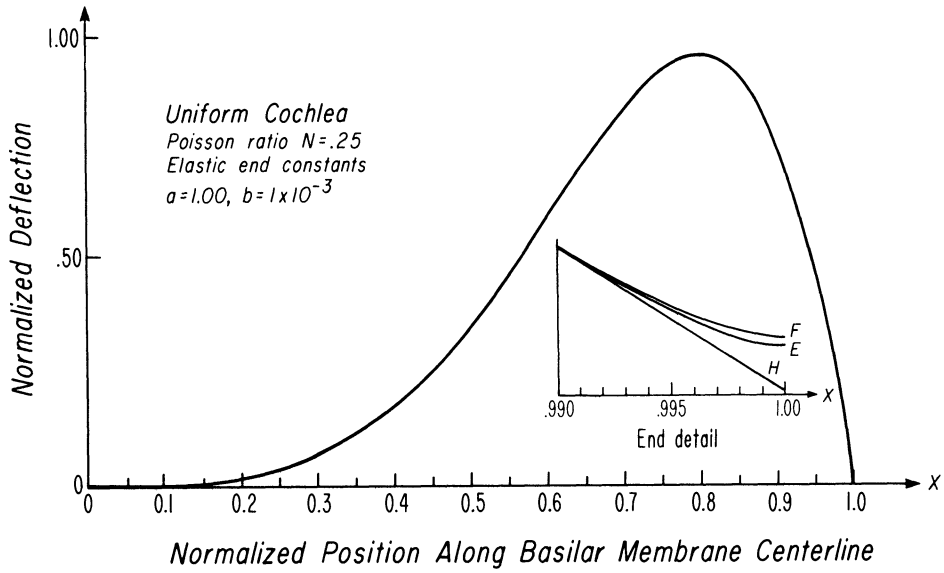

FIG. 14. *Deflection of the basilar membrane's centerline (BMC) as* $\omega \to 0$ *for a uniform (cylindrical) cochlea.*

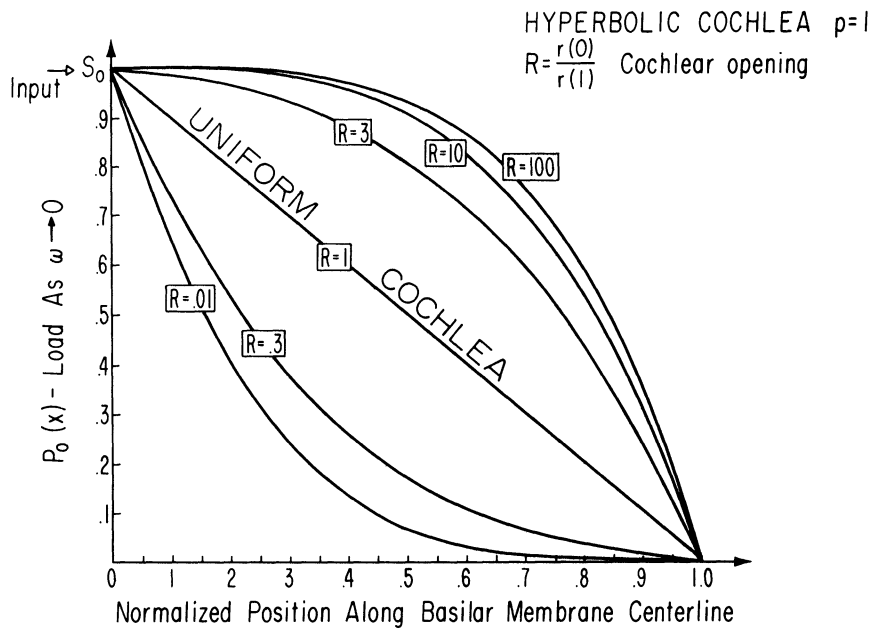

FIG. 15. *Induced loads on the basilar membrane as* $\omega \to 0$ *due to hyperbolic cochleas.*

This can be seen in Fig. 16 where the resulting deformations of the BMC are plotted. When $R = 3$, $x_{M0} \sim .83$ for all end conditions. Surprisingly, it looks as if increasing R further does not have much effect on x_{M0}. This is better illustrated in Fig. 17 where, for $p = 1$, we see that $.5 < x_{M0} < .84$ for all R. The lower bound is even more surprising. It means that no matter how much the cochlea widens (when $p = 1$) as $R \to 0$, x_{M0} does not become arbitrarily small. In the corresponding curve for $p = 1/3$

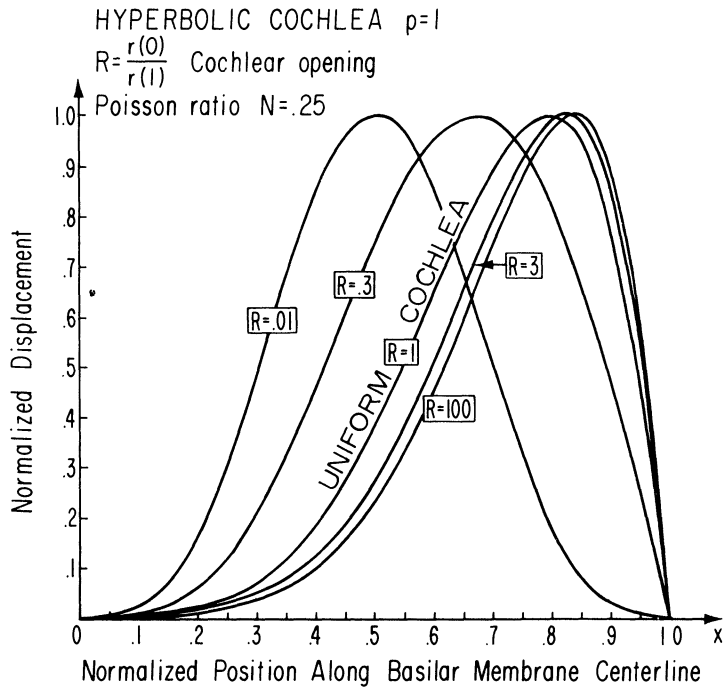

FIG. 16. *Deflections of the BMC as* $\omega \to 0$ *for hyperbolic cochleas. Compare with the induced loads in Fig.* 15.

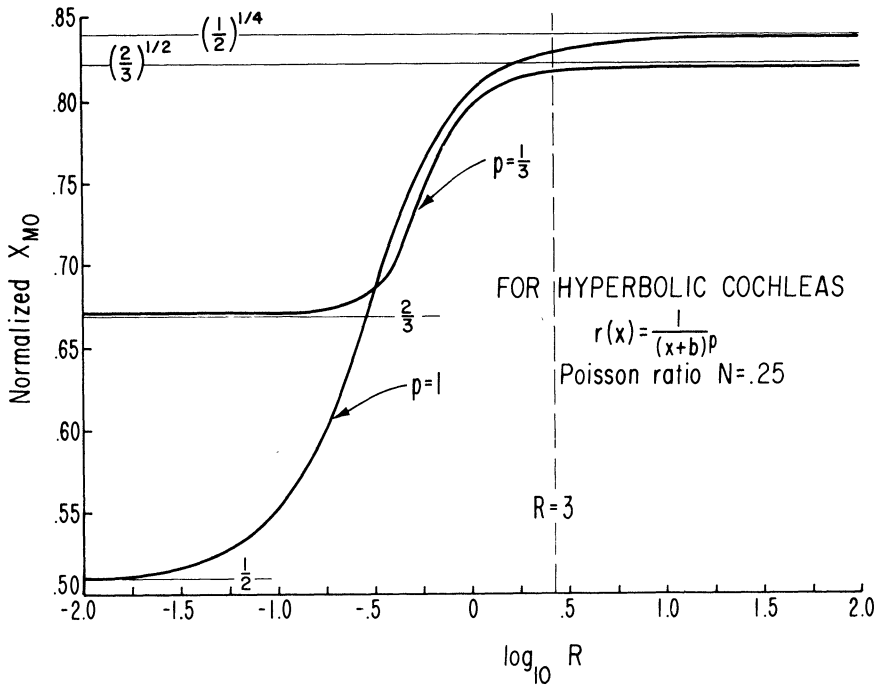

FIG. 17. *Range of* x_{M0}, x_{max} *as* $\omega \to 0$, *as geometry varies in hyperbolic cochleas. See also Fig.* 19.

we have $.66 < x_{M0} < .825$. To understand how the cochlea's geometry affects x_{M0} requires a bit more care.

For a given p and $r(0)$, the cochlear radius at the origin, we define:

(i) the *widest* cochlea as that having $R = 0$ (i.e., $r(1) \to \infty$) and

(ii) the *narrowest* cochlea as that having $R = \infty$ (i.e., $r(1) = 0$). We establish that for each p

$$\frac{4}{3p+5} \leqq x_{M0} \leqq \left(\frac{4}{3p+5}\right)^{1/(3p+1)}, \tag{95}$$

the lower bound found when $R = 0$ and the upper bound when $R = \infty$.

For a load

$$p_0(x) = cx^n, \tag{96a}$$

we find the corresponding particular solution of the deflection equation

$$a_{0_p}(x) = \frac{2cx^{n+4}}{[m^2-(n+2)^2][m^2-(n+4)^2]}, \tag{96b}$$

which for $m \gg n$, as in our case, is very accurately approximated by

$$a_{0_p}(x) = \frac{2c}{m^4}x^{n+4}. \tag{96c}$$

Since a_{0_p} is linear in p_0, from (96) we can immediately synthesize a_{0_p} for any polynomial p_0. Further for $x < 1$ the contribution of a_{0_c} (see (80)), for all coefficients A and C given in § 3.2.3, is so absolutely insignificant that the deflection is very accurately given by

$$a_0(x) = a_{0_p}(x), \qquad x < 1. \tag{97}$$

For hyperbolic cochleas we have:

(i) the narrowest cochlea is given by $d = 0$ and induces a load (suppressing the constant S_0)

$$p_0(x) = (1 - x^{3p+1}).$$

From (96c) and (97) the BMC deflection is

$$a_0(x) = \frac{2}{m^4}(x^4 - x^{3p+5}).$$

We find directly by differentiation that

$$x_{M0} = \left(\frac{4}{3p+5}\right)^{1/(3p+1)}$$

which gives the upper bound in (95).

(ii) The widest cochlea is when $d = -1$ inducing the load

$$p_0(x) = \frac{(x-1)^{3p+1}}{(-1)^{3p+1}}.$$

We use the binomial theorem to expand this load and subsequently applying (96) termwise we get the deflection

$$\frac{m^4}{2}a_0(x) = \frac{1}{(-1)^{3p+1}} \sum_{r=0}^{3p+1} C_r^{3p+1}(-1)^r x^{3p+5-r}.$$

To find x_{M0} we differentiate $a_0(x)$ and set the result equal to zero obtaining

$$\sum_{r=0}^{3p+1} C_r^{3p+1}(-1)^r(3p+5-r)x^{3p+1-r} = 0. \tag{98}$$

Actually, this nasty looking polynomial can be nicely factored into

$$(x-1)^{3p}[(3p+5)x-4]. \tag{99}$$

Expanding (99) we have

$$\begin{aligned}
&[(3p+5)x-4]\left(\sum_{r=0}^{3p} C_r^{3p}(-1)^r x^{3p-r}\right) \\
&= (3p+5)x^{3p+1} + \sum_{r=1}^{3p} C_r^{3p}(-1)^r(3p+5)x^{3p+1-r} - 4\sum_{r=0}^{3p-1} C_r^{3p}(-1)^r x^{3p-r} + 4(-1)^{3p+1} \\
&= (3p+5)x^{3p+1} + \sum_{r=1}^{3p} (-1)^r\{C_r^{3p}(3p+5) + 4C_{r-1}^{3p}\}x^{3p+1-r} + 4(-1)^{3p+1} \\
&= (3p+5)x^{3p+1} + \sum_{r=1}^{3p} (-1)^r C_r^{3p+1}(3p+5-r)x^{3p+1-r} + 4(-1)^{3p+1} \\
&= \sum_{r=0}^{3p+1} (-1)^r C_r^{3p+1}(3p+5-r)x^{3p+1-r}
\end{aligned}$$

which establishes our assertion.

Replacing the polynomial in (98) by (99) we immediately find that

$$x_{M0} = \frac{4}{3p+5}$$

which provides the lower bound in (95).

Actually the equality signs in (95) are somewhat doubtful since we used approximations in the proof. Note, however, that for $p = 0$, $R = 1$ and we have the uniform cochlea. From (95) we get $x_{M0} = \frac{4}{5}$ as an upper and lower bound, which is also the computed result.

The meaning of (95) is pictorialized in Fig. 18. The implication is clear, for realistic values of p (say less than 2) and $R \sim 3$, the narrowing of the cochlea and the basilar membrane's taper are not enough to push x_{M0} to 1. What's missing?

Let's take another look at the human cochlea (particularly Fig. 2). Uncoiled it looks somewhat like Fig. 19 with *three* chambers, rather than the two chambers we have considered so far. The middle chamber (cochlear duct) plays a crucial role at very low frequencies.

In two-chamber models the net pressure on the basilar membrane's apical end is the *same* as the net pressure at the adjacent helicotrema. There, with the possible exception of some slight friction losses, we have unimpeded fluid flow. Hence the pressures just above and below the helicotrema balance (pressure equalization), ergo the zero net pressure stated in boundary condition (29). With three chambers, however, the net pressure (let's call it $p_{\text{net}}(1)$) along the edge $x = 1$ of the basilar membrane is *not* zero since the basilar membrane is shielded from the helicotrema by Reissner's membrane. Consequently, $p_{\text{net}}(1)$ is the difference between the pressures at $x = 1$ (see detail C in Fig. 19), in the scala tympani and *cochlear duct* (rather than the scala vestibuli as is the case in a two chambered cochlea). A preliminary study of a

three-chambered cochlea [74] showed that

$$p_{\text{net}}(1) \sim .3S_0$$

where S_0 is the input pressure from the stapes at $x = 0$. For this reason the constant P is introduced in condition (66). We write

(100) $$p_{\text{net}}(1) = PS_0$$

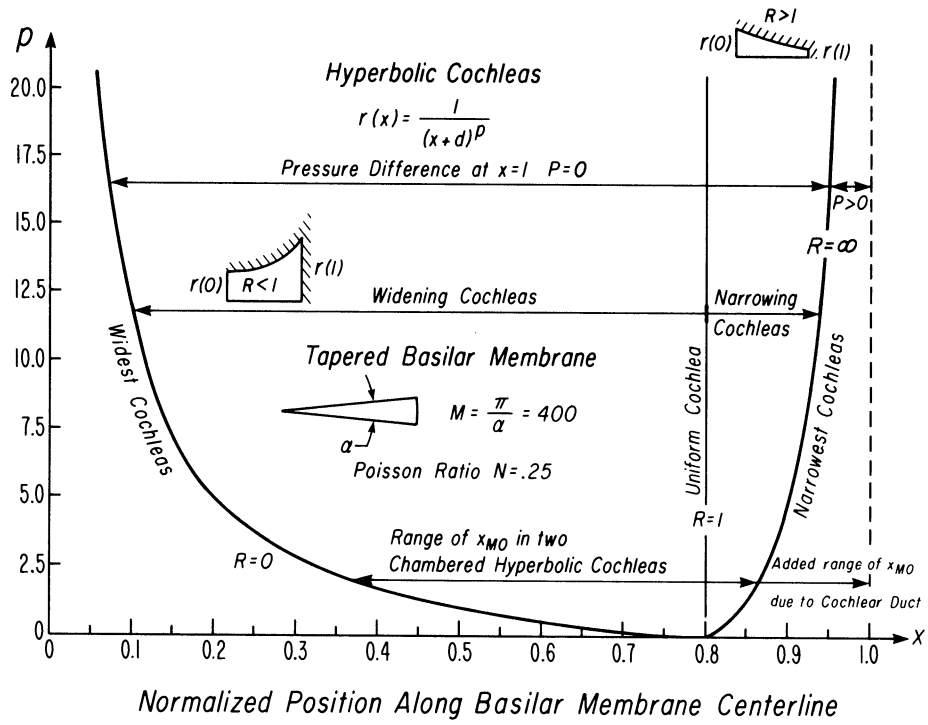

FIG. 18. *Summary of results for hyperbolic cochleas. Range of x_{M0} between curve for narrowest cochleas and $x = 1$ corresponds to quasi-three-chambered models.*

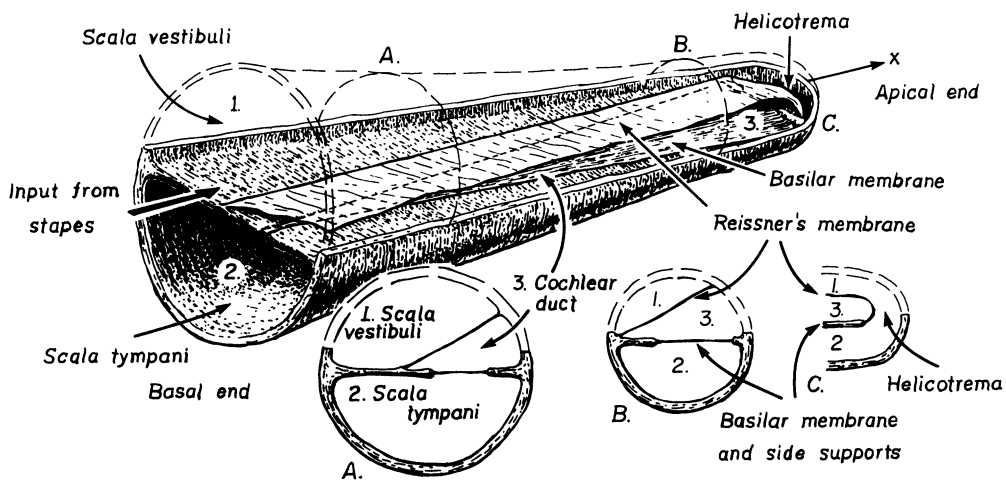

FIG. 19. *Three-chambered uncoiled cochlea. A and B are cross sections, while C is a longitudinal section.*

where P is a constant somewhat larger than .3 to allow for small friction losses in the fluid flow. With this condition the model may be called "quasi-three-chambered," since at least as $\omega \to 0$, it accounts for the effects of the cochlear duct.

When $R = 3$ and $p = 1$ the difference in $p_0(x)$ due to the presence of the cochlear duct is shown in Fig. 20. The additional load is, in fact, needed to bring x_{M0} to the vicinity of $x = 1$. And this fact, as we will see, unveils a beautiful surprise. The basilar

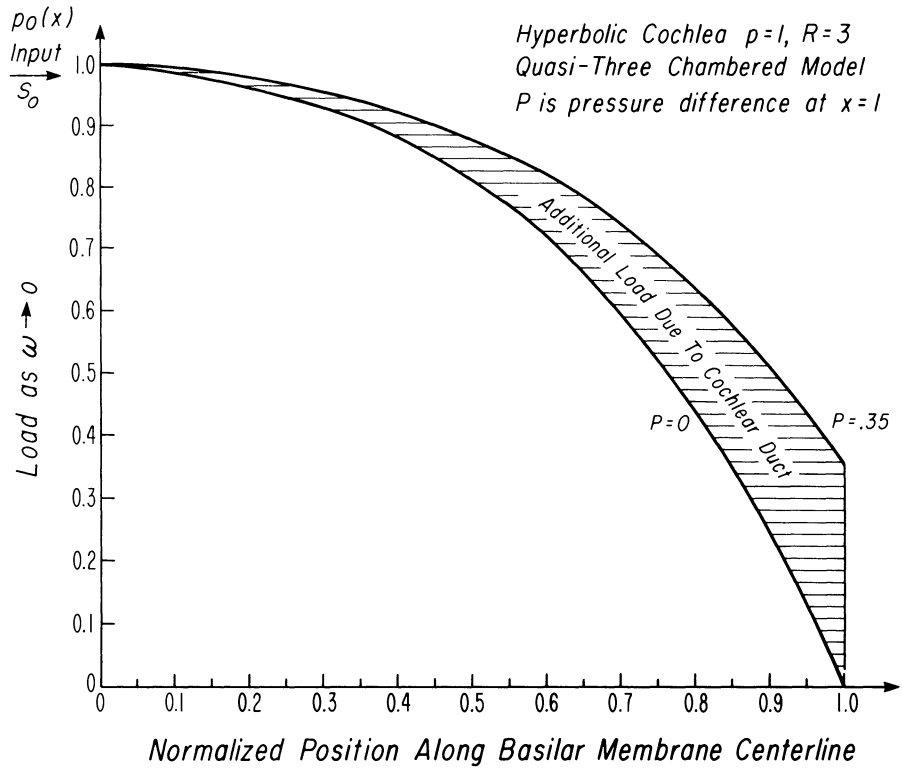

FIG. 20. *Load on the basilar membrane as $\omega \to 0$ induced by two-chambered and quasi-three-chambered hyperbolic cochleas.*

membrane's deflection for a quasi-three-chambered cochlea is shown in Fig. 21. The x_{M0} now being very close to $x = 1$ depends on the boundary conditions there. As long as x_{M0} was far from $x = 1$ the constraint there did not affect it. With (100), however, the problem of proper boundary conditions at the apical end must be settled. A glance at Fig. 5 shows that the basilar membrane can move at $x = 1$. This utilizes the membrane's full length for frequency discrimination. For, if the basilar membrane was simply supported at $x = 1$ (conditions (82)), then $x_{M0} \sim .98$ (see Fig. 21) and the last 2% or so of the membrane's length would be "wasted," in the sense that no peaking could occur there. Leaving the basilar membrane unconstrained (free end conditions (85)) at $x = 1$, Fig. 21 shows that $x_{M0} = 1$. Yet something is wrong. The deformation does not look like that displayed in Fig. 5 (say for 25 cps). In the last $\frac{1}{2}$% of its length the membrane's tail end flaps like a flag. Such a spirited oscillation would surely tear the membrane. What might be the reason that this does not happen?

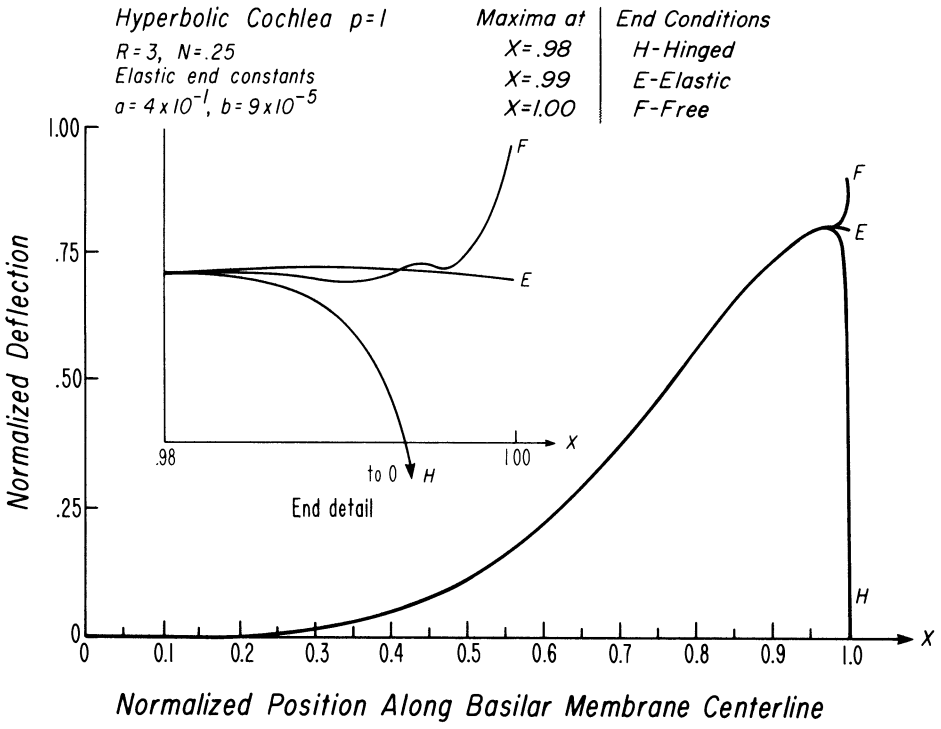

FIG. 21. *Deflection of the BMC as* $\omega \to 0$ *for various boundary conditions at the apical end* ($x = 1$) *in a quasi-three-chambered hyperbolic cochlea. Notice the flapping of the free-end.*

Prompted by this inquiry, Dr. Fred Linthicum of the Ear Research Institute in Los Angeles looked at the basilar membrane's apical end under the electron microscope and saw a previously unnoticed microstructure. Within the last $\frac{1}{2}$% of its length, the basilar membrane becomes noticeably more fibrous, and, further, a rather strong ligament along $x = 1$ constrains its motion there, and prevents it from flapping and tearing.

We perceive, then, the motivation for including an elastic end as one of the boundary conditions ((88) and (89) yielding the coefficients (92) and (93)) at $x = 1$. For, with this constraint and a hyperbolic cochlea with $p = 1$ we obtain $x_{M0} \sim .99$ (Fig. 21), without any flapping.

To study more arbitrary cochlear geometries a computer program based on this model was constructed [99]. There, cochlear shapes are defined by means of spline functions [100] and the induced load on the basilar membrane and its resulting deformation are computed. Figs. 22 and 23 illustrate the versatility of this approach. For one of the cochlear shapes $x_{M0} = 1.00$ as in Fig. 5. That program is being used by medical researchers at the Ear Research Institute of Los Angeles in an attempt to understand better those hearing pathologies due to mechanical defects in the cochlea.

3.4. Epilogue. Recall the stipulation in § 2.3.4, that frequency thresholds are characterized by diminished sensitivity (i.e., $dx_{\max}/d\omega \to 0$), and a small maximum amplitude, i.e., $|\eta(x_{\max})| \leqq k$) as well. The two-dimensional model with uniform geometry, as we have seen, yields excellent high frequency behavior:

$$\lim_{\omega \to \infty} dx_{\max}/d\omega = 0 \quad \text{and} \quad x_{\max} \downarrow 0 \quad \text{as } \omega \to \infty$$

with

$$\lim_{\omega \to \infty} \eta(x_{\max}) = 0.$$

Earlier (at the end of § 1.2), we saw that our findings on the high-frequency threshold enabled us to offer an explanation for the causes of presbycusis (diminished high frequency hearing with aging). Our results regarding the mechanism of low

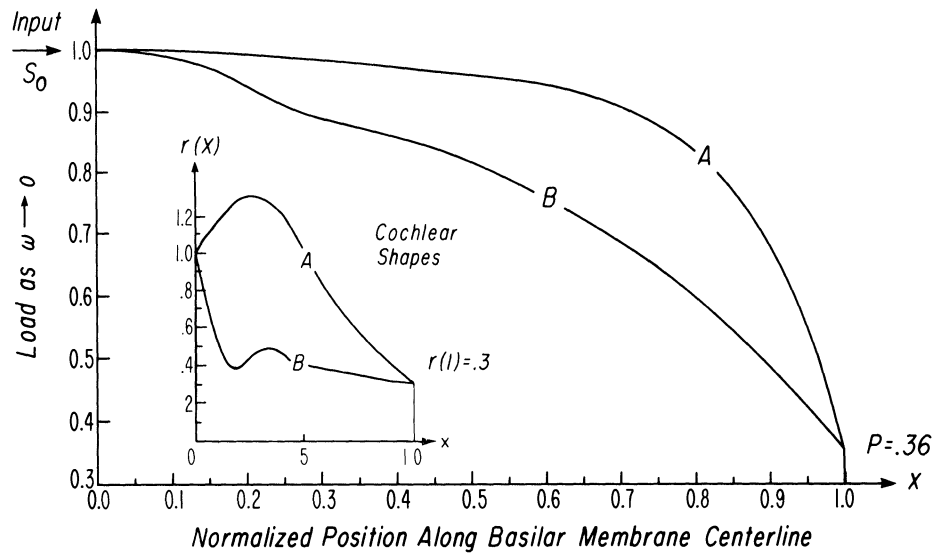

FIG. 22. *Loads as $\omega \to 0$ induced by the indicated cochlear shapes (surfaces of revolution generated by rotating curves A and B about the x-axis).*

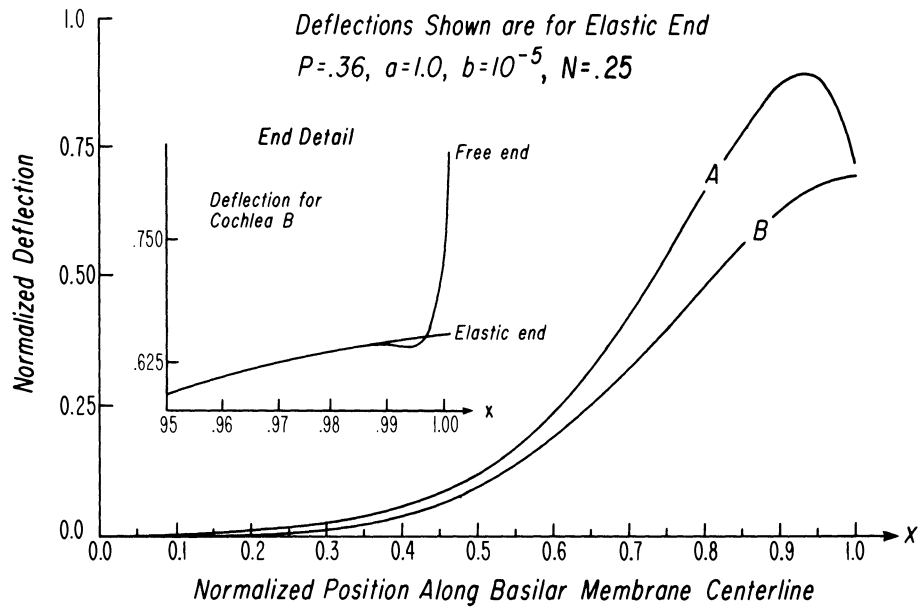

FIG. 23. *Deflections of the BMC as $\omega \to 0$ for cochlear shapes shown in Fig. 21. Again notice the flapping of the free-end.*

frequency hearing are supported by the symptoms of a pathology called Meniere's syndrome. Typically, in this pathology, an excessive amount of fluid accumulates in the cochlear duct (③ in Fig. 19), substantially increasing the load on the basilar membrane and other cochlear structures. The resulting distortions should, according to our findings, affect primarily low frequency hearing. This, in fact, is observed clinically. Additionally, this affliction often results in buzzing, ringing, and other high frequency sound originating within the ear. Based on our results, we may speculate on the causes of this phenomenon. Perhaps the deformed cochlea, unlike its normal counterpart, can resonate (see § 2.3.1), triggered by some normally unnoticed sound, thus creating the sensation. Or, possibly, the additional load overloads our ligament at $x = 1$ and causes a mild flapping that drives the cochlear fluids so that they behave as if a high frequency signal had been introduced.

To complete our summary, we found that the low frequency threshold turned out to be far more elusive than the high frequency threshold due to the intricate interaction of the geometry, the effect of the cochlear duct, and the boundary conditions at the apical end. In the two dimensional model

$$\lim_{\omega \to 0} dx_{\max}/d\omega = 0, \tag{101a}$$

and in the quasi-three-chambered model, we found a configuration for which

$$\lim_{\omega \to 0} x_{\max} = x_{M0} = 1. \tag{101b}$$

But, to determine rigorously whether (101a), (101b), and

$$\begin{aligned} &x_{\max} \uparrow 1, \\ &|\eta(x_{\max})| \leqq k \quad \text{as } \omega \to 0 \end{aligned} \tag{101c}$$

are true, requires the solution of the equations of motion for the three-dimensional model, at least in a neighborhood of $\omega = 0$. As well, estimates for the bounding constant k could be obtained from physical measurements of the constraining constants a and b due to the end ligament.

The roles of the main structural features of the cochlea are now qualitatively better understood. The solution of some of the problems stemming from this work, and outlined in the following section, will provide a quantitative understanding of cochlear dynamics. Then, a meaningful comparison between model predictions and experimental data can ensue.

4. Research problems.

4.1. It is worthwhile to know whether a place principle holds for *all* positive input frequencies in the last model. This is equivalent to asking if $x_{\max}$ is a continuous and monotone decreasing function of ω, for $\omega \in [0, \infty)$. One might be tempted to study this problem from the equations of motion ((54), (61) and (62)), and use qualitative arguments, rather than attempt to solve the equations directly.

A word of caution. Since $x_{\max}$ is also a function of the physical properties of the system, a place principle may exist only in a restricted range of the model parameters. This was the case in the first and second models (see also the pertinent discussion in [62]).

4.2. A more ambitious undertaking is to solve the equations, subject to the given side conditions, for all positive input frequencies, and subsequently, to analyze the

solution function ($\eta = \eta(x, t, \omega)$) as is done for the second model (§ 2). As an added variant, either the equations of motion should be reformulated to include the higher modes of the basilar membrane's oscillations (see end of § 3.1), or it should be rigorously shown that the higher modes can be safely neglected.

4.3. Develop a model for a three-chambered cochlea [74]. As in two-chambered models, start with a set of equations of motion of the perilymph in the scala vestibuli (see Fig. 19), and another set of equations for the motion of the perilymph in the scala tympani. The boundary conditions should include the fact that these flows communicate through the helicotrema and friction losses may occur there.

A separate set of equations of motion describes the flow—generated by the energy transmitted at the boundaries—of the endolymph in the cochlear duct sac. The flows in the scala vestibuli and cochlear duct interact through Reissner's membrane which enters as the connecting moving boundary between the two chambers. Note that Reissner's membrane is offset and has a nearly rectangular shape (for a treatment of Reissner's membrane see [101]). Since it is very thin, its motion—at least initially—would be adequately described by a two-dimensional wave equation for a rectangular membrane. The cochlear duct and scala tympani interact through the basilar membrane whose motion, as we have seen, should be described by the plate equation.

The boundary condition for the net pressure in the fluid at the helicotrema should differ, for the reasons explained in § 3, from the net pressure condition across the apical end of the basilar membrane (see Fig. 19c).

4.4. Consider also that almost all cochleas—in the various species—are coiled. Therefore, two-chambered as well as three-chambered cochlear models should be developed in some sensible helical coordinate system. Only in recent years have there been attempts to cope with this very difficult aspect of cochlear geometry [61], [63] and [72].

4.5. Develop (two- or three-chambered, straight or coiled) cochlear models *without* a wavelength assumption.

Nearly all mathematical models, including those given here, contain in their formulation an assumption about the "typical" wavelength—long or short—of the basilar membrane's oscillation (see annotated bibliography in the appendix). Such an assumption is not really justified. Most probably both "long" and "short" wavelength oscillations of the basilar membrane occur. The basic reason for using a wavelength assumption is to eliminate some terms from the equations of motion.

4.6 It would be an appealing contribution to dynamics to delimit the bare essentials of all mechanical systems exhibiting a place principle under periodic forcing (i.e., theorems providing necessary and sufficient conditions for systems having a place principle).

Perhaps then, cochlear dynamics could be viewed as a particular "optimization" problem. Specifically, let an elastic plate (the "basilar membrane"), of length L, be immersed in a viscous and incompressible fluid and enclosed by a rigid structure (the "cochlea" appropriately partitioned). We would like such a system to exhibit the place principle between a low frequency threshold at ω_L and a high frequency threshold at ω_M. We would like, as well, to find the properties (ν, E, ρ, geometry, etc.) of the system such that

$$\text{(i)} \quad x_{\max} \downarrow \text{ continuously for } \omega \in [\omega_L, \omega_M]$$

and

$$\text{(ii)} \quad L = \left[\lim_{\omega \to \omega_L} x_{\max}, \lim_{\omega \to \omega_M} x_{\max}\right].$$

The first requirement is simply that the system exhibit a place principle in its audio range $[\omega_L, \omega_M]$. In (ii) we require that the system optimize its sensitivity to frequency discrimination (i.e., maximize the spread of frequencies along the available length). Intuitively, it seems that such an approach could provide fascinating information on the evolution of the cochlea in the various species.

4.7. Still another intriguing problem deals with fine pitch discrimination. Though the place principle gives tonal localization, it does not sufficiently explain the fine frequency discrimination of the auditory system. In general, the envelopes of η are not sufficiently sharp in the neighborhood of their maximum to allow for accurate distinction between the $x_{\max}$ for a frequency ω and $x_{\max}$ for a frequency $\omega + \Delta\omega$ ($\Delta\omega$ small). Consequently, it has been conjectured [102] that the auditory nerve "processes" the mechanical information in the neighborhood of $x_{\max}$ by performing sharpening transformations, and thus "creates" the perceptions of $x_{\max}$ that occur. A good theory of sharpening transformations and sharpening networks (i.e., networks of elements imitating the sharpening neural function) is still not available. Those who wish to pursue this problem can begin with [103], [15], [104].

4.8. In this study (§ 2), we solved a set of partial differential equations (the equations of motion) in order to get the time-envelopes of the oscillation η. An interesting question naturally arises: is it possible to obtain the envelopes directly and bypass the laborious solution process? The properties of envelopes of the solution function of a set of partial differential equations are of interest in many applications.

One might proceed by generalizing the notion of envelopes. More precisely, let

$$z = f(x_1, \cdots, x_m)$$

be a function of m independent variables. Intuitively, consider the hyper-surface Z_{m-n} of dimension $m-n$, generated as a specified subset of $n < m$ independent variables approach their extreme values. Z_{m-n} is the generalization of the notion of envelopes with respect to *one* variable. (For an old, but pleasing, treatment of the theory of envelopes see Osgood [105].) If z is a function satisfying a set of partial differential equations, with sufficient side conditions, when can an algorithm be found for obtaining the envelope Z_{m-n} of z directly from the partial differential equations? At the outset, one might try to find the time-envelope η_E, of η, for the second model equations (27), (28) and (29). Or, even better, one might derive an equation for the time-envelope of η and find $x_{\max}$ directly. A successful outcome might lead to a generalization of the procedure. This approach would illuminate a crucial problem: how is frequency discriminated when the input consists of combination tones? Specifically, given the input

$$\text{(102)} \qquad \sum_{i=1}^{k} A_i \sin \omega_i t,$$

how are the individual frequency components $\omega_1, \cdots, \omega_k$ distinguished? If we had an equation for the envelopes, we might find the nonlinear superposition rules (see [16], [17]) that apply to the synthesis of the composite envelope of (105) in terms of the individual envelopes of

$$A_i \sin \omega_i t.$$

Let us close with a few words on methodology. We have seen that this study is permeated with small parameters (e.g., small basilar membrane displacement, thin boundary layer, slender cochlea geometry). We can exploit the powerful methods of asymptotic analysis in the study of cochlear mechanics by formalizing these observations. Already, Professor L. Rubenfeld has suggested that the results on high and low frequencies (i.e., as $\omega \to \infty$, and as $\omega \to 0$) could more easily be derived by using asymptotics. Further, we have dealt exclusively with symmetric cochlear models. Using perturbation techniques, many "small" asymmetries in cochlear geometry could be included in the models. Such a study has, in fact, been initiated by Professor C. Coleman, R. Finley, and others at Harvey Mudd College. Additionally, pathologies could be considered as perturbations of the normal.

Using dimensional analysis, scaling laws for the cochlea could be derived (e.g., notice the numerous dimensional groups of parameters that arose in the first, second and third models). This would enable utilization of the data from mechanical models as well as data from comparative physiology for the various species.

Appendix

ANNOTATED SURVEY OF A CENTURY OF COCHLEAR MODELING

BY PAUL NEISWANDER†

The highlights, rather than the totality, of each researcher's work are emphasized. Among the various models the meaning of many cochlear parameters is nonuniform and occasionally obscure. Therefore, comparisons between models without checking the original sources are hazardous. All references in the survey, cited by author and year of publication, are listed in the bibliography.

In the remarks, statements such as "b.m. stiffness decreases exponentially" refer to variations with distance from the stapes. The long (or short) wavelength assumption refers to the "average" wavelength of the b.m.'s oscillation being large (or small) when compared to the average height of the cochlear chamber. With the long-wave assumption the transverse (across the b.m.) fluid motion is negligible, the fluid equations are one-dimensional and the cochlea may be modeled by simple electrical ladder networks using a volt-pressure analogy. In short-wave models the transverse fluid motion must be considered. Discussion abounds on the implications of these assumptions (i.e., Zwislocki [55, (1950)], Steele [69, (1974)] and Siebert [73, (1974)]). Finally, except for Huxley [61, (1969)] and Lieberstein [63, (1971)], all models surveyed have an uncoiled cochlea.

1869 Helmholtz (mathematical).

Cochlea: Not considered.

Perilymph: Provides uniform pressure on b.m.

B.m.: Semi-infinite wedge-shaped membrane with no longitudinal tension and uniform transverse tension (array of uncoupled resonators or "strings").

Solution: Analytic.

Results: Demonstrates a place principle without true longitudinal wave motion. Introduction of an earlier (and less accurate) version of this model in 1857 marked the beginning of modern auditory theory (Wever [18, *Theory of Hearing*, p. 25]).

1903 Ewald (mechanical). Demonstrates b.m. standing waves, confirming Ewald's "acoustic image" theory of hearing (Wever [18, p. 45]). This model was a precursor to von Békésy's cochlear models.

† IBM Los Angeles Scientific Center, Los Angeles, California 90045.

1924 Wegel and Lane (electrical). The first electrical ladder network analogy of the cochlea. The parameter values were unknown at the time so no solutions were found.

1928 von Békésy (mechanical).

Cochlea: Brass and glass frame with two uniformly tapered chambers, including helicotrema. Oval and round windows covered with rubber membranes.

Perilymph: Glycerin and water in life-size models, water in larger models.

B.m.: Uniformly tapered rubber membranes in metal frames (similar to Ewald's though stiffer).

Results: Observation with microscope, stroboscopic illumination. Demonstrates the place principle (as it is currently accepted), traveling waves and eddy pairs localized near the maximum of b.m. displacement ("Békésy's eddies"). These phenomena agree qualitatively with his observations in three-chamber models and in cadaver ears.

Von Békésy's Nobel prize-winning investigation of hearing began with these model studies (see von Békésy [22, *Experiments in Hearing*, p. 404]).

1930 Kucharski (mathematical). An advanced long-wave two-chamber model (see Zwislocki [21, (1953)]).

1930 Fletcher (mathematical). Based on a theory in which each point of the b.m. resonates with a frequency determined by the local stiffness and the mass of a fluid column connecting that point to the oval window.

1933 Reboul (mathematical). Long-wave model with one chamber. Predicts b.m. phase velocity would increase from base to apex (see Zwislocki [21]).

1947 De Rosa (mathematical). Long-wave two-chamber model of structurally uniform cochlea with compressible perilymph. Assumes place principle based on constructive interference patterns of fast and slow pressure waves.

1948 Zwislocki (mathematical).

Cochlea: Two chambers with constant cross-sectional area. Helicotrema neglected. No round window impedance.

Perilymph; Incompressible, viscous.

B.m.: Array of mechanically uncoupled resonators. Stiffness decreases exponentially. Mass neglected. Resistance constant. Assumes long wavelengths.

Solution: Analytic.

Results: Good agreement with von Békésy's b.m. amplitude-frequency curves. This is the first "modern" mathematical model (Licklider [19, (1953)]). See Zwislocki [55, (1950)] for an English description and Zwislocki [59, (1965)] for an interesting extension.

1950 Ranke (mathematical).

Cochlea: Two chambers with constant height, infinite width. Helicotrema neglected.

Perilymph: Incompressible, inviscid.

B.m.: Array of mechanical uncoupled resonators, resonant frequency decreasing exponentially. 'Q' constant. Assumes short wavelengths.

Solution: Analytic.

Results: Agreement with von Békésy's b.m. amplitude-frequency curves, predicts minimum b.m. phase velocity. Until Siebert [73, (1974)], Ranke was the only proponent of the short-wave assumption. See Ranke [52, (1950)] for a final version of his model and Ranke [54, (1950)] for a summary of his arguments and for a comparison of b.m. waves with breaking surf.

1950 Peterson and Bogert (mathematical).

Cochlea: Two chambers with uniformly tapered cross-sectional area. Pressure equalization at the helicotrema. No round window impedance.

Perilymph: Compressible, inviscid.

B.m.: Array of mechanically uncoupled resonators. Stiffness decreases exponentially. Mass constant. Resistance neglected. Width increases uniformly. Assumes long wavelengths.

Solution: Semi-analytic.

Results: Demonstrates place principle with infinite maxima (since the model was lossless) above 50 hz. This was the first successful American model and formed the basis for many subsequent papers. Bogert [38, (1951)] added b.m. resistance to an electrical analogue of this model, smoothing the maxima.

1951 Fletcher (mathematical). Long-wave model essentially the same as those of Zwislocki and Peterson and Bogert except for a more detailed treatment of cochlear parameters (i.e., viscous and inertial losses in the helicotrema). Solution by numerical integration. Good agreement with von Békésy's b.m. amplitude-frequency curves.

1956 Bauch (electrical). Ladder network based on Zwislocki's model, showing the effect of b.m. mass insignificant.

1958 Tonndorf (mechanical).

Cochlea: Lucite enclosures with two and three chambers. Helicotrema included.

Perilymph: Glycerin and water solutions.

B.m.: Tapered rubber membranes with various stiffness gradients.

Results: Observations with microscope, stroboscopic illumination, motion pictures. In Tonndorf [31, (1958)] and subsequent papers (see Tonndorf [32, (1970)]), models demonstrate the place principle, traveling waves, shearing motions in the b.m., von Békésy's eddies, nonlinear beat phenomena and asymmetrical b.m. motion.

1960 Flanagan (mathematical). No details of cochlear mechanics considered. This model is an empirical transfer function fitting von Békésy's b.m. response curves, with applications to transient response middle ear impedance effects and psychoacoustic phenomena (see Flanagan [58, (1962)]).

1961 Oetinger and Hauser (electrical). Ladder network based on lengthy mathematical derivation. Stiffness of oval and round windows included.

1966 Klatt and Peterson (electrical). Ladder network (see Klatt [41, (1964)]) with applications to transient response and middle ear impedance effects. Steady state response also found by computer.

1969 Huxley (mathematical). Long-wave model of an infinitely long, lossless, two-chamber cochlea. Four cases of b.m. mechanical coupling considered: (1) none, (2) longitudinal tension, (3) longitudinal rigidity, (4) longitudinal rigidity with curvature effects. Concludes that b.m. standing-wave resonance (all points move in phase) is possible only in the fourth case.

1970 Inselberg and von Foerster (mathematical).

Cochlea: Not considered.

Perilymph: Provides concentrated driving moment at basal end of b.m., viscous damping of b.m.'s motion.

B.m.: Uniform beam, simply supported at both ends.

Solution: Analytic.

Results: Demonstrates place principle and simultaneous occurrence of traveling and standing (transient) waves. High and low frequency "thresholds." Fluid properties important at high frequencies, geometry at low frequencies.

1971 Lieberstein (conceptual). Nonmathematical extension of the model of Inselberg and von Foerster. B.m. analyzed as a spiraling narrow plate clamped on all

edges. Resulting vibrational modes principally transverse as opposed to the longitudinal modes of a beam. Local regions of plate vibrate quasi-independently, leading to Helmholtz-type place principle.

1972 Lesser and Berkley (*mathematical*).

Cochlea: Two chambers with constant cross-sectional area. Helicotrema neglected.

Perilymph: Incompressible, inviscid.

B.m.: Array of mechanically uncoupled resonators. Stiffness and resistance exponentially decreasing. Mass constant. No assumption of wavelength size.

Solution: Semi-numerical, employing fast Fourier transforms.

Results: Shows the necessity of considering details of transverse fluid motion. Mechanical model demonstrates two time scales of fluid motion: a short scale in which the mathematical model is valid, and a long scale in which nonlinear effects develop.

1972 Stewart (*mathematical*). Computer simulation of electrical ladder network (see Stewart [100, (1967)]) derived from topological considerations rather than mathematical theory. Circuit interpreted as series of low-pass filters.

1972 Geisler and Hubbard (*electrical*). Analogue computer circuit (see Hubbard and Geisler [44, (1972)]) yielding solutions to the Peterson–Bogert equations with round window stiffness included. Results indicate (1) a frequency-independent transmembrane pressure at base does not correspond to constant pressure at oval window, and (2) the perilymph cannot be assumed incompressible above 7 kHz.

1973 Schroeder (*mathematical*). Long-wave model (similar to those of Zwislocki and Peterson and Bogert) based on the assumptions that local b.m. resonant frequency and phase velocity decrease exponentially and local 'Q' is constant. Analytic solution. Results indicate high-frequency b.m. amplitude drop (at fixed position) is related solely to the number of wavelengths on the b.m. at low frequencies. See Schroeder [27, (1975)] for an interesting elaboration.

1973 Kim, Molnar and Pfeiffer (*mathematical*). System of differential equations representing b.m. as an array of uni-directionally coupled resonators with nonlinear resistances. Parameters empirical. Results compare with observed nonlinear phenomena.

1974 Steele (*mathematical*).

Cochlea: Two semi-infinite wedge-shaped chambers (constant height) with vertex at stapes (taper opposite to that in real cochlea). Helicotrema neglected.

Perilymph: Incompressible, viscosity introduced as perturbation effect.

B.m.: Two b.m. models considered: (1) semi-infinite wedge-shaped plate, (2) the first model with stiffer rods of Corti along one edge. No assumption of wavelength size.

Solution: Method of solution not given in detail. Includes phase-integral and perturbation methods.

Results: Shows short-wave approximation valid near maximum of b.m. displacement, which occurs about 5 mm farther from stapes than maximum displacement of the rods of Corti.

1974 Viergever and Kalker (*mathematical*). The first part of this paper extended the Peterson–Bogert model to the three dimensions and shows the one-dimensional model inadequate at high frequencies. The second part discusses von Békésy's eddies as the major effect of viscosity.

1974 Soroka (*mechanical*). Two-chamber model 30× life size. Rubber b.m. with tension decreasing towards apex. Observation with electromagnetic pickup. Results indicate the relation of b.m. elasticity and inertia (rather than relation of viscosity and

inertia) determines b.m. response.

1974 Allaire, Raynor and Billone (*mathematical*). Model of b.m. as a series of composite transverse beams. Shows greater stiffness under high frequency loads than low frequency or static loads. Also shows nonlinear stiffening.

1974 Helle (*mechanical*). Two-chamber model, 30× life size, with simulated tectorial membrane (see Zwicker [35, *Facts and Models in Hearing*, p. 77]). Shows a possible fine-tuning mechanism related to the closing of a normally open gap between the organ of Corti and the tectorial membrane (due to streaming).

1974 Zwicker (*mechanical*). Three-chamber model of 5 mm segment of cochlea 200× life size, with simulated tectorial membrane (see Zwicker [35, *Facts and Models in Hearing*, p. 95]). Shows a possible fine-tuning mechanism related to the opening of a normally closed gap between the organ of Corti and the tectorial membrane (due to streaming).

1974 Siebert (*mathematical*). The first short-wave model since Ranke's. Discussion includes "paradoxical waves" (see Siebert [64, (1971)] and von Békésy [22, *Experiments in Hearing*, p. 510]), and a suggestion that the high dispersion inherent in short-wave models might be corrected by including b.m. mechanical coupling.

1974 Hall (*electrical*). Ladder network with nonlinear b.m. resistance. Demonstrates combination tones.

1975 Chadwick, Israeli and Levite (*mathematical*). Long-wave model introducing the third chamber (scala media). Results indicate that if Reissner's membrane were about as stiff as the b.m. then there can be two b.m. maxima at a given frequency (contradicting the currently accepted place principle).

1975 Novoselova (*mathematical*). Model of the b.m. as an anisotropic thin plate. Results show linear behavior at low and moderate sound intensities. Von Békésy's b.m. amplitude-frequency data were extrapolated to the linear region, showing agreement with more recent data.

1975 Chadwick and Adler (*mechanical*). Two-chamber model using combinations of water or glucose (for the perilymph) and rubber or steel (for the b.m.) to verify the mathematical model of Inselberg et al. [76, 77, (1976)] and to investigate the effects of viscosity. Optical lever system used for observation.

1976 Inselberg, Chadwick and Johnson (*mathematical*).

Cochlea: Two chambers with constant cross-section. Pressure equalization at helicotrema. No round window impedance.

Perilymph: Incompressible, viscous (thin boundary layers).

B.m.: Uniform beam. Assumed long wavelengths.

Solution: Analytic.

Results: This extension of the model of Inselberg [62, (1970)] confirms and improves the previous results. Place principle good at high frequencies and poor at low frequencies. Shows that b.m. stiffness gradient is needed for good low-frequency response. High and low frequency "thresholds."

1976 Zweig, Lipes and Pierce (*mathematical*). Long-wave model similar to Schroeder [67, (1973)]. Results indicate the cochlea is optimized with regard to conflicting requirements of (1) traveling waves without reflections and (2) accurate frequency analysis. Relates high-frequency b.m. amplitude slope to b.m. losses as well as to number of wavelengths on b.m. (see Schroeder's model).

1976 van Dijk (*mathematical*). Uses conformal mappings to transform a two-dimensional cochlea to a simple geometry. Three integral equations found (but not solved) for assumptions of long, short and all wavelengths.

1977 Inselberg (*mathematical*).

Cochlea: Quasi-three-chambered. Arbitrary surface of revolution partitioned into two symmetric chambers. Due to cochlear duct (third chamber) there is a pressure difference at helicotrema.

Perilymph and endolymph: Viscous and incompressible.

B.m.: Isotropic uniform thickness sector-shaped plate. Simple supports along long edges with three different boundary conditions at apical end.

Solution: Analytic at low frequencies.

Results: Explains role of cochlear cross section taper and opposing b.m. taper. Shows that cochlear duct is needed for optimal utilization of b.m. as a frequency analyzer. Shows that b.m. needs elastic support at apical end.

Acknowledgments. It is a pleasure to acknowledge my debt to numerous colleagues, friends and organizations for valuable assistance in the course of this work.

The IBM Corporation, through its Los Angeles Scientific Center (LASC), has graciously and unselfishly supported this research. Messrs. W. Wangel, J. Hinchcliffe and G. Rathe of IBM as well as Drs. H. H. Givin, L. Leeburg, B. Dimsdale and A. Hurwitz of IBM–LASC have, in several ways, capably and consistently given time and contributed considerable skill.

For their insightful suggestions and encouragement, I am indebted to Henry Scarton and Lester Rubenfeld of Renssalear Polytechnic Institute. As well, I enjoyed and deeply benefited from my collaboration with the Ear Research Institute of Los Angeles, especially in the persons of Drs. Fred Linthicum, William House and Jack Pulec.

I am grateful to Ephraim Shaket who wrote the programs and did the computations for § 3, to Paul Neiswander for valuable discussions and his considerable labors resulting in the Annotated Survey, to Marvin Klotz for his editorial labors, to Vicky Jones who made the beautiful drawings in Figs. 13 and 19, and to Jean Sells who drew the other figures.

It is impossible to acknowledge fully my gratitude to my charming and inspiring teacher, Professor Heinz von Foerster of the University of Illinois. A long time ago he opened my eyes—and ears—with his innovative and exciting research.

REFERENCES

[1] H. L. F. VON HELMHOLTZ, *Sensations of Tone*, Dover, New York, 1954. (Republication of the second (1885) edition of the Ellis translation of *Die Lehre von den Tonempfindungen*, originally published by Longmans & Co., London.)

[2] ———, *Treatise on Physiological Optics*, 1886, English transl. of first German edition, Optical Society of America, 1924.

[3] A. J. LOTKA, *Elements of Physical Biology*, 1928, reissued as *Elements of Mathematical Biology*, Dover, New York, 1956.

[4] V. VOLTERRA, *Leçons sur la Théorie Mathématique de la Lutte pour la Vie*, Gauthier-Villars, Paris, 1931.

[5] N. RASHEVSKY, *Mathematical Biophysics*, vols. 1 and 2, third ed., Dover, New York, 1960.

[6] H. L. RESNIKOFF, *Differential geometry and color perception*, J. Math. Biol., 1 (1974), pp. 97–131.

[7] R. THOM, *Structural Stability and Morphogenesis*, Addison-Wesley, Reading, MA, 1974. (Translated by D. H. Fowler from the French edition and updated by author.)

[8] E. C. ZEEMAN, *The geometry of catastrophe*, The Times Literary Supplement, 10 Dec. 1971.

[9] G. W. SWAN, *A Bibliography in Mathematical Biology*, S. Levin, ed., *Mathematical Problems in Biology* (Victoria Conference), Lecture Notes in Biomathematics, No. 2, Springer-Verlag, New York, 1974.

[10] R. THOM, *Local topological properties of differentiable mappings*, Bombay Colloquium on Differentiable Analysis, Oxford University Press, Oxford, 1964.

[11] ———, *Topological models in biology*, Topology, 8 (1969), pp. 313–335.

[12] J. CALLAHAN, *Singularities and plane maps*, Amer. Math. Monthly, 81 (1974), pp. 211–240.
[13] W. S. MCCULLOCH AND W. PITTS, *A logical calculus of the ideas immanent in nervous activity*, Bull. Math. Biophys., 5 (1943), pp. 115–133.
[14] ———, *How we know universals; The perception of auditory and visual forms*, Ibid., 9 (1947), pp. 127–147.
[15] H. VON FOERSTER, *Computation in neural nets*, Currents Mod. Biology, 1 (1967), pp. 47–93.
[16] A. INSELBERG, *Superpositions for nonlinear operators: I. Strong superpositions and linearizability*, J. Math. Anal. Appl., 40 (1972), pp. 494–508.
[17] ———, *Superpositions for nonlinear operators: II. Generalized affine operators*, Ibid., 41 (1973), pp. 260–269.
[18] E. G. WEVER, *Theory of Hearing*, John Wiley, New York, 1949.
[19] J. LICKLIDER, *Hearing*, Ann. Rev. Psychol., 4 (1953), pp. 89–110.
[20] E. G. WEVER AND M. LAWRENCE, *Physiological Acoustics*, Princeton University Press, Princeton, NJ, 1954.
[21] J. ZWISLOCKI, *Review of recent mathematical theories of cochlear dynamics*, J. Acoust. Soc. Amer., 25 (1953), pp. 743–751.
[22] G. VON BÉKÉSY, *Experiments in Hearing*, McGraw-Hill, New York, 1960.
[23] T. S. LITTLER, *The Physics of the Ear*, Macmillan, New York, 1965.
[24] J. V. TOBIAS, *Foundations of Modern Auditory Theory*, vols. I and II, Academic Press, New York, 1970–1972.
[25] P. DALLOS, *The Auditory Periphery*, Academic Press, New York, 1973.
[26] A. MØLLER, ed., *Basic Mechanics in Hearing*, Academic Press, New York, 1973.
[27] M. SCHROEDER, *Models of hearing*, Proc. IEEE, 63 (1975), pp. 1332–1350.
[28] *Journal of the Acoustical Society of America.*
[29] J. R. EWALD, *Zur Physiologie des Labyrinths, VII, Mitt., Die Erzengung von Schallbildern in der camera acustica*, Pflüg. Arch. ges. Physiol., 93 (1903), pp. 485–500.
[30] G. VON BÉKÉSY, *Zur Theorie des Hörens; Die Schwingungs form der Basilarmembran*, Physik. Zeits., 9 (1928), pp. 793–810 (see von Békésy, *Experiments in Hearing*, pp. 404–429).
[31] J. TONNDORF, *Harmonic distortion in cochlear models*, J. Acoust. Soc. Amer., 30 (1958), pp. 929–937.
[32] ———, *Nonlinearities in cochlear hydrodynamics*, Ibid., 47 (1970), pp. 574–578.
[33] L. A. SOROKA, *Hydrodynamic modelling of the inner ear*, Soviet Phys. Acoust, 19 (1974), pp. 565–568.
[34] R. HELLE, *Selektivitätssteigerung in einem hydromechanischen Innenohrmodell mit Basilar- und Deckmembran*, Acustica, 30 (1974), pp. 301–312 (see Zwicker, *Facts and Models in Hearing*, Springer-Verlag, New York, 1974, pp. 77–85.
[35] E. ZWICKER, *Ein hydromechanisches Ausschnittmodell des Innenohres zur Erforschung des adäquaten Reizes der Sinneszellen*, Acustica, 30 (1974), pp. 313–319 (see Zwicker, *Facts and Models in Hearing*, Springer-Verlag, New York, 1974, pp. 95–99).
[36] R. CHADWICK AND D. ADLER, *Experimental observations of a mechanical cochlear model*, J. Acoust Soc. Amer., 58 (1975), pp. 706–710.
[37] R. L. WEGEL AND C. C. LANE, *The auditory masking of one pure tone by another and its possible relation to the dynamics of the inner ear*, Phys. Rev., 23 (1924), pp. 266–285.
[38] B. P. BOGERT, *Determination of the effects of dissipation in the cochlear partition by means of a network representing the basilar membrane*. J. Acoust Soc. Amer., 23 (1951), pp. 151–154.
[39] H. BAUCH, *Die Schwingungsform der Basilarmembran bei Erregung durch Impulse und Geräusche, gemessen an einem elektrischen Modell des Innenohres*, Frequenz, 10 (1956), pp. 222–234.
[40] R. OETINGER AND H. HAUSER, *Ein elektrischer Kettenleiter zur Untersuchung der mechanischen Schwingungsforgäng im Innenohr*, Acustica, 11 (1961), pp. 161–177.
[41] D. KLATT, *Theories of aural physiology*, Communication Sciences Lab Report 13, Univ. of Michigan, Ann Arbor, MI, 1964.
[42] D. KLATT AND G. PETERSON, *Reexamination of a model of the cochlea*, J. Acoust. Soc. Amer., 40 (1966), pp. 54–61.
[43] A. HUBBARD AND C. GEISLER, *A hybrid-computer model of the cochlear partition*, Ibid., 51 (1972), pp. 1895–1903.
[44] C. GEISLER AND A. HUBBARD, *New boundary conditions and results for the Peterson–Bogert model of the cochlea*, Ibid., 52 (1972), pp. 1629–1634.
[45] J. HALL, *Two-tone distortion products in a non-linear model of the basilar membrane*, Ibid., 56 (1974), pp. 1818–1828.
[46] H. L. F. VON HELMHOLTZ, *Appendix XI* in [1]. Also presented as *On acoustical vibrations of the labyrinth of the ear*, Lecture in naturh.-med. verein. of Heidelberg, 25 June 1869.

[47] VON W. KUCHARSKI, *Schwingungen von membranen in eirer pulsierenden flüssigkeit*, Physik Zeits., 31 (1930), pp. 264–280.
[48] H. FLETCHER, *A space-time pattern theory of hearing*, J. Acoust. Soc. Amer., 1 (1930), pp. 311–343.
[49] J. A. REBOUL, *Théorie des phénomènes mécaniques se passant dans l'oreille interne*, J. de Physique, 9 (1938), pp. 185–194.
[50] L. DE ROSA, *A theory as to the function of the scala tympani in hearing*, J. Acoust Soc. Amer., 19 (1947), pp. 623–628.
[51] J. ZWISLOCKI, *Die Theorie der Schneckenmechanik*, Acta-Oto-Laryn., Supp. 72 (1948).
[52] O. F. RANKE, *Hydrodynamik der Schnecken flüssigkeit*, Zeits. für Biol., 103 (1950), pp. 409–434.
[53] L. C. PETERSON AND B. P. BOGERT, *A dynamical theory of the cochlea*, J. Acoust. Soc. Amer., 22 (1950), pp. 369–381.
[54] O. F. RANKE, *Theory of operation of the cochlea: a contribution to the hydrodynamics of the cochlea*, J. Acoust. Soc. Amer., 22 (1950), pp. 772–777.
[55] J. ZWISLOCKI, *Theory of the acoustical action of the cochlea*, Ibid., 22 (1950), pp. 778–784.
[56] H. FLETCHER, *On the dynamics of the cochlea*, Ibid., 23 (1951), pp. 637–645.
[57] J. L. FLANAGAN, *Models for approximating basilar membrane displacement*, Bell System Tech. J., 39 (1960), pp. 1163–1191.
[58] ———, *Computational model for basilar membrane displacement*, J. Acoust. Soc. Amer., 34 (1962), pp. 1370–1376.
[59] J. ZWISLOCKI, *Analysis of some auditory characteristics*, Handbook of Mathematical Psychology, Volume III, Luce, Bush and Galanter, eds., John Wiley, New York, 1965.
[60] J. STEWART, *Speech processing with a cochlear-neural analog*, AMRL-TR-66-229, Aerospace Medical Res. Lab., Wright-Patterson AFB, Ohio, 1967.
[61] A. F. HUXLEY, *Is resonance possible in the cochlea after all?*, Nature, 221 (1969), pp. 935–940.
[62] A. INSELBERG AND H. VON FOERSTER, *A mathematical model of the basilar membrane*, J. Math. Biosc., 7 (1970), pp. 341–363.
[63] M. LIEBERSTEIN, *The basilar membrane as a uniformly loaded plate clamped on two spiral boundaries in a plane or on two helical-spiral boundaries*, Ibid., 12 (1971), pp. 281–291.
[64] W. SIEBERT, *'Paradoxical' waves, bone conduction, and cochlear models*, MIT Electronics Res. Lab. Quarterly Report 1971, 100, pp. 214–221.
[65] M. LESSER AND D. BERKLEY, *Fluid mechanics of the cochlea, Part 1*, J. Fluid Mech., 51 (1972), pp. 497–512.
[66] J. STEWART, *A theory and physical model for cochlear mechanics*, Acta-Oto-Laryn., Supp. 294, 1972.
[67] M. SCHROEDER, *An integrable model for the basilar membrane*, J. Acoust Soc. Amer., 53 (1973), pp. 429–434.
[68] D. KIM, C. MOLNAR AND R. PFEIFFER, *A system of non-linear differential equations modelling basilar membrane motion*, Ibid., 54 (1973), pp. 1517–1529.
[69] C. STEELE, *Behavior of the basilar membrane with pure-time excitation*, Ibid., 55 (1974), pp. 148–162.
[70] M. VIERGEVER AND J. KALKER, *On the adequacy of the Peterson-Bogert model and on the effects* of viscosity in cochlear dynamics, J. Engr. Math., 8 (1974), pp. 149–156.
[71] P. ALLAIRE, S. RAYNOR AND M. BILLONE, *Cochlear partition stiffness—a composite beam model*, J. Acoust. Soc. Amer., 55 (1974), pp. 1252–1258.
[72] M. H. LIEBERSTEIN AND J. A. RICKARD, *The basilar membrane as a set of uniformly loaded circular annular plates clamped on both edges*, J. Math. Biosc., 21 (1974), pp. 339–344.
[73] W. SIEBERT, *Ranke revisited—a simple short-wave cochlear model*, J. Acoust. Soc. Amer., 56 (1974), pp. 599–600.
[74] R. CHADWICK, M. ISRAELI AND U. LEVITE, *Virtual mass and damping corrections to a one-dimensional formulation of cochlear mechanics with an application to a three chamber model*, Israel J. Tech., 13 (1975), pp. 168–179.
[75] S. M. NOVOSELOVA, *The basilar membrane as an elastic plate*, Soviet Phys. Acoust., 21 (1975), pp. 56–60.
[76] A. INSELBERG AND R. CHADWICK, *Mathematical model of the cochlea, I: Formulation and solution*, SIAM J. Appl. Math., 30 (1976), pp. 149–163.
[77] R. CHADWICK, A. INSELBERG AND K. JOHNSON, *Mathematical model of the cochlea, II: Results and conclusions*, Ibid., 30 (1976), pp. 164–179.
[78] G. ZWEIG, R. LIPES AND J. PIERCE, *The cochlear compromise*, J. Acoust. Soc. Amer., 59 (1976), pp. 975–982.

[79] J. VAN DIJK, *On the hydrodynamics of the inner ear, Theoretical part. A mathematical model*, Acustica, 35 (1976), pp. 190–201.
[80] A. INSELBERG, *Quasi-three-chambered model of the cochlea*, to be submitted for publication.
[81] B. JOHNSTONE AND A. BOYLE, *Basilar membrane vibration examined with the Mössbauer technique*, Science, 158 (1967), pp. 389–390.
[82] W. RHODE, *Observations of the vibration of the basilar membrane in squirrel monkeys using the Mössbauer technique*, J. Acoust. Soc. Amer., 49 (1971), pp. 1218–1231.
[83] L. ROBLES, W. RHODE AND C. D. GEISLER, *Transient response of the basilar membrane measured in squirrel monkeys using the Mössbauer effect*, Ibid., 59 (1976), pp. 926–939.
[84] L. KOHLLÖFFEL, *A study of basilar membrane vibrations, I, II, III*, Acustica, 27 (1972), pp. 49–89.
[85] J. WILSON AND J. JOHNSTONE, *Basilar membrane and middle-ear-vibration in guinea pig measured by capacitive probe*, J. Acoust. Soc. Amer., 57 (1975), pp. 705–723.
[86] J. WILSON, *Basilar membrane vibration data and their relation to theories of frequency analysis*, Facts and Models in Hearing, E. Zwicker and E. Terhardt, eds., Springer-Verlag, New York, 1974, pp. 56–64.
[87] J. ZWISLOCKI, *Cochlear waves: interaction between theory and experiments*, J. Acoust. Soc. Amer., 55 (1974), pp. 578–583.
[88] C. D. GEISLER AND A. E. HUBBARD, *The compatibility of various measurements on the ear as related by a simple model*, Acustica, 33 (1975), pp. 220–222.
[89] A. INSELBERG, *Dynamics of the basilar membrane*, in progress report on the res. on the analyzing principles of the mammalian auditory system # 1–10 cont. # AF33(616)-6428, Electr. Engr. Res. Lab., Univ. of Illinois, Urbana, 1959–1960.
[90] G. K. BATCHELOR, *An Introduction to Fluid Dynamics*, Cambridge University Press, Cambridge, 1967.
[91] J. ZWISLOCKI, *Analysis of the middle-ear function, Part I: Input impedance*, J. Acoust. Soc. Amer., 34 (1962), pp. 1514–1523.
[92] A. R. MØLLER, *Transfer function of the middle ear*, Ibid., 35 (1963), pp. 1526–1534.
[93] J. W. GRANT, *Biomechanics of the semicircular canals*, Ph.D. Thesis, Dept. of Mechanical Engineering, Tulane Univ., New Orleans, 1973.
[94] P. NEISWANDER, *Computer simulation of the ear*, M.Sc. Thesis, Dept. of Physics, California State Univer. Los Angeles, 1975.
[95] P. W. WHALEY, *An acoustic impedance meter and its value as a diagnostic tool*, Ph.D. Thesis, Mechanical Engineering Dept., Oklahoma State University, 1975.
[96] L. B. W. JOLLEY, *Summation of Series*, Dover, New York, 1961.
[97] S. TIMOSHENKO AND S. WOINOWSKY-KRIEGER, *Theory of Plates and Shells*, McGraw-Hill, New York, 1959.
[98] J. LIGHTHILL, *Mathematics of aquatic animal locomotion at low Reynolds number*, Mathematical Biofluiddynamics, Society for Industrial and Applied Mathematics, Philadelphia, 1975, Chap. 3.
[99] A. INSELBERG, *Variable geometry cochlea model at low frequency input*, IBM J. Res. Develop., 21, (1977), pp. 461–478.
[100] ———, *Cubic splines with infinite derivatives at some knots*, Ibid., 20 (1976), pp. 430–436.
[101] C. R. STEELE, *Stiffness of Reissner's membrane*, J. Acoust. Soc. Amer., 56 (1974), pp. 1252–1257.
[102] W. H. HUGGINS AND J. C. R. LICKLIDER, *Place mechanisms of auditory frequency analysis*, Ibid., 23 (1951), pp. 290–299.
[103] A. INSELBERG AND H. VON FOERSTER, *Linear property filters* (NSF Grant 17414) Tech. Rep. 2, Electr. Engr. Res. Lab., Engr. Exper. Station, Univ. of Illinois, Urbana, 1962.
[104] M. CONRAD, *Evolutionary learning circuits*, J. Theor. Biol., 46 (1974), pp. 167–188.
[105] W. F. OSGOOD, *Advanced Calculus*, Macmillan, New York, 1962, pp. 186–194.